Ultrathin Films of Single-Walled Carbon Nanotubes for Electronics and Sensors: A Review of Fundamental and Applied Aspects

By *Qing Cao* and *John A. Rogers**

Ultrathin films of single-walled carbon nanotubes (SWNTs) represent an attractive, emerging class of material, with properties that can approach the exceptional electrical, mechanical, and optical characteristics of individual SWNTs, in a format that, unlike isolated tubes, is readily suitable for scalable integration into devices. These features suggest the potential for realistic applications as conducting or semiconducting layers in diverse types of electronic, optoelectronic and sensor systems. This article reviews recent advances in assembly techniques for forming such films, modeling and experimental work that reveals their collective properties, and engineering aspects of implementation in sensors and in electronic devices and circuits with various levels of complexity. A concluding discussion provides some perspectives on possibilities for future work in fundamental and applied aspects.

1. Introduction

Single-walled carbon nanotubes (SWNTs) are, by now, a well-known class of material. Their molecular structure can be visualized as graphene sheets rolled-up to certain directions designated by pairs of integers (Fig. 1a). Interest in SWNTs derives from the exceptional electrical, mechanical, optical, chemical, and thermal properties associated with their unique quasi 1D structure, atomically monolayered surface, and extended curved π-bonding configuration.[1–6] An individual SWNT can be either semiconducting, metallic or semimetallic, depending on its chirality and diameter. These different types of SWNTs can be contemplated for use as active channels of transistor devices, due to their high mobilities (up to $\sim$10 000 cm^2 Vs^{-1} at room temperature),[7] or as conductors for advanced electrical interconnects, due to their low resistivities,[8–11] high current-carrying capacities (up to $\sim 10^9$ A cm^{-2}),[12] and high thermal conductivities (up to 3500 Wm^{-1} K^{-1}).[13] In addition, SWNTs are stiff and strong, exhibiting Young's moduli in the range of 1–2 TPa, as inferred from properties of bundles and multiwalled tubes[14–19] or, recently, as determined directly from measurements on statistically significant sets of isolated SWNTs.[20] The fracture stresses can be as high as 50 GPa, as determined from SWNT bundles,[21,22] yielding a density-normalized strength $\sim$50 times larger than that of steel wires.[18] Although structurally perfect SWNTs are chemically inert due to the absence of surface dangling bonds,[23,24] their properties can be very sensitive to adsorbed species, partly because of weight-normalized surface areas as high as 1600 m^2 g^{-1},[25] thereby rendering them attractive for various sensor applications. Over the past decade, large numbers of academic and industrial groups have explored the use of SWNTs in diverse application possibilities, ranging from nanoscale circuits for beyond silicon based complementary metal-oxide-semiconductor (CMOS) era electronics,[26–28] to low voltage, cold-cathode field-emission displays,[29] to hydrogen-storage devices,[30–32] to agents for drug delivery,[33,34] to light-emitting devices,[35,36] thermal heat sinks,[37,38] electrical interconnects,[39] and chemical/biological sensors.[40]

The electronic properties of SWNTs are among their most important features. Use as an electronic material represents one of their most commonly envisioned areas of application. Their high mobilities and ballistic transport characteristics, for example, have led naturally to their consideration as a replacement for Si in future generation devices, especially when continued dimensional scaling as the primary driver for improved performance becomes increasingly difficult.[28,41–43] Unlike other proposed "future" electronic technologies, such as spintronics,[44–47] molecular electronics,[48–53] quantum-dot cellular automata,[54] and nanowire crossbar arrays,[55–60] SWNTs have the advantage of being compatible with conventional field-effect transistor (FET) architectures. Experimental data suggest that SWNTs offer more than one order of magnitude improvement in device transconductance over Si technology for otherwise similar designs, together with small intrinsic capacitance for possible operation at terahertz frequencies (Fig. 1b).[28,42,61,62] Despite many notable achievements in devices constructed on individual SWNTs, such

[*] Q. Cao, Prof. J. A. Rogers
Department of Chemistry
Department of Materials Science and Engineering
Department of Electrical and Computer Engineering
Department of Mechanical Science and Engineering
Beckman Institute
Frederick-Seitz Materials Research Laboratory
University of Illinois at Urbana-Champaign Urbana, IL 61801 (USA)
E-mail: jrogers@uiuc.edu

DOI: 10.1002/adma.200801995

as the realization of a three-stage CMOS ring oscillator based on a single tube (Fig. 1c),[63] there are many daunting challenges in scaling to any realistic type of system. The two most important of these are the inability to draw significant current output from single SWNT devices, and the lack of practical methods to yield good device-to-device reproducibility in properties. This second challenge arises from an absence of techniques for synthesis of electronically homogeneous SWNTs, and of methods to form them with controlled orientations and spatial locations.

Systems that involve large numbers of nanotubes in random networks, aligned arrays, or anything in between, and with thicknesses between sub-monolayer and a few layers, avoid these challenges. Many believe that SWNTs in these formats offer the most technologically realistic integration path, at least for the foreseeable future. In particular, because many SWNTs are involved in transport in such ''films,'' they offer i) attractive statistics that minimize device-to-device variations even with electronically heterogeneous tubes, ii) large active areas and high current outputs, and iii) relative insensitivity to spatial position or orientation of individual tubes. In optimized layouts that consist of perfectly aligned arrays of long tubes, these films can exhibit properties that approach those associated with isolated SWNTs.[64] As a result, these materials have some potential for use in high-frequency electronics, possibly heterogeneously integrated with CMOS Si platforms.[65] Even in completely random networks, which are easy to synthesize, the characteristics can be attractive.[66] Such SWNT films can facilitate new types of applications in electronics that are enabled by large area coverage (i.e., macroelectronics[67]), mechanical flexibility/stretchability, or optical transparency. This review summarizes recent progress in this relatively new field, with an emphasis on advanced demonstrations in electronics and sensors. The first section reviews methods for assembling SWNT thin films. After a summary of experimental and theoretical work on the nature of charge transport in these systems, various implementations in sensors and in electronic devices, e.g., thin-film transistors (TFTs), and digital/analog circuits are presented. The final section concludes with some perspectives on opportunities for future work.

John A. Rogers obtained B.A. and B.S. degrees in chemistry and in physics from the University of Texas, Austin, in 1989. From MIT, he received S.M. degrees in physics and in chemistry in 1992 and a Ph.D. in physical chemistry in 1995. He currently holds the Flory-Founder Chair in Engineering at the University of Illinois at Urbana-Champaign. Rogers' research includes fundamental and applied aspects of nanometer- and molecular-scale fabrication, materials and patterning techniques for unusual format electronics and photonic systems.

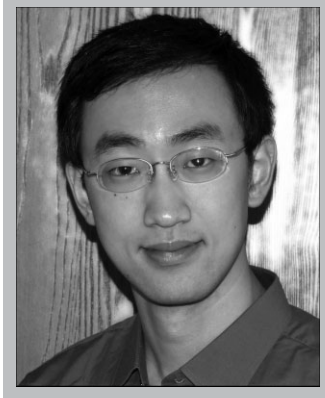

Qing Cao was born in 1983 in China. He received a B.Sc. degree in Chemistry from Nanjing University in 2004. He then came to the United States and is currently a Ph.D. candidate in Materials Chemistry working under direction of Professor John A. Rogers at the University of Illinois at Urbana-Champaign. His research interests include functional nanomaterials, micro/nanofabrication, as well as materials and device design for unconventional electronic systems.

2. Preparation of Carbon-Nanotube Films

Formation of films of SWNTs with coverages ranging from sub-monolayer to a few layers on desired substrates represents the starting point for their fundamental study and use in applications. The fabrication techniques must provide control over the tube density (*D*, as measured in the number of tubes per unit area for random network films or tubes per length for aligned arrays), the overall spatial layouts of the SWNT, their lengths, and their orientations. These parameters significantly influence the collective electrical, optical, and mechanical properties. Some ability to control the diameter distributions and, ideally, the ratio of semiconducting to metallic SWNTs (*m*-SWNTs) can also be important. For certain applications mentioned in the introduction, these methods should also be compatible with large areas and low-cost processing. This section describes some of the most successful approaches.

2.1. Solution Deposition Methods

Techniques to form SWNT thin films by depositing tubes separately synthesized by one of several bulk methods from solution suspensions are attractive because they can be cost-effectively scaled to large areas and they are compatible with a wide variety of substrates. A successful strategy generally involves a reliable means, such as surfactant wrapping, to form stable solutions of SWNTs, and a robust mechanism to remove them from solution, such as through evaporation of solvent,[68,69] or specific interactions between nanotubes, ligands, or surfaces.[70–75] In perhaps the simplest approach, known as the vacuum-filtration method, vacuum-induced flow of a suspension of SWNTs through a porous filtration membrane leaves SWNTs trapped on the surface of the filter, to provide control over *D* in certain ranges.[69,76] The vacuum helps to remove solvent and to increase the overall throughput. This method is widely used for in assembling high-*D* multilayered SWNT films for applications as transparent conductive coatings, discussed in Section 4. An obvious limitation is that the SWNTs deposit on filter membranes, which are not generally substrates of interest.

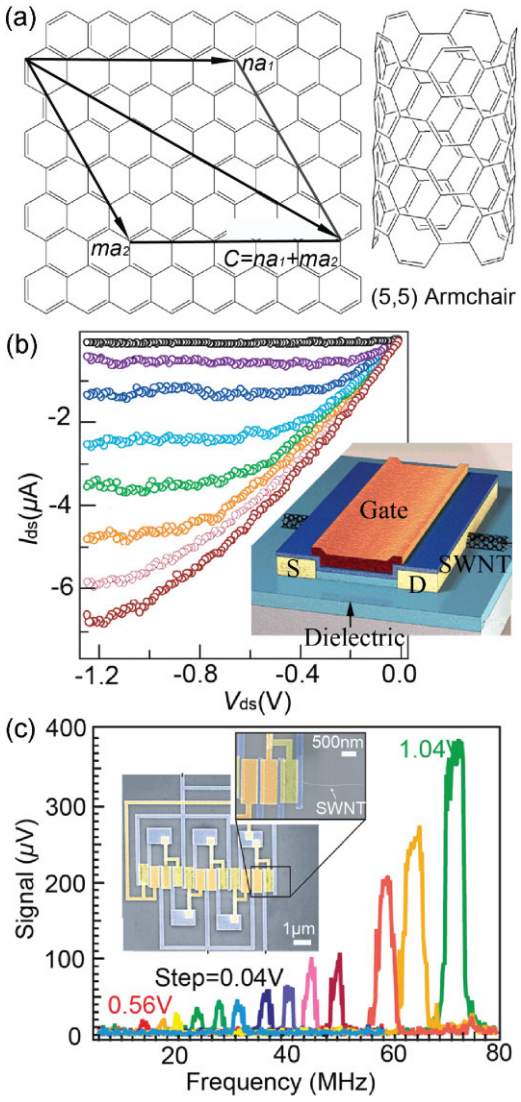

Figure 1. a) Formation of a SWNT by rolling a graphene sheet along a chiral vector *C*, such as the (5,5) vector shown here. b) Current–voltage characteristics of an FET constructed on a single SWNT, with a high *k* dielectric (V_{GS}: Gate-source voltage changed from 0.3 to 1 V in steps of 0.1 V from bottom to up; I_{DS}: drain-source current; V_{DS}: drain-source voltage). Reproduced with permission from Ref. [61]. Copyright 2002 Nature Publishing Group. Inset: Schematic view of the device layout. Reproduced with permission from Ref. [1]. Copyright 2002 American Chemical Society. c) Oscillation frequency under different supply voltages changed from 0.56 to 1.04 V in steps of 0.04 V for a three-stage CMOS ring oscillator constructed on a single SWNT. Inset: SEM image of the tube and circuit structures. Reproduced with permission from Ref. [63]. Copyright 2006 The American Association for the Advancement of Science (AAAS).

Certain transfer techniques, described subsequently, can address this issue.[77] A practical challenge for solution deposition methods is that the low solubility and strong intertube interactions of SWNTs make it difficult to obtain sub-monolayer SWNT thin films, with uniform moderate-to-high coverage (i.e., high *D*) and without significant presence of bundles. The use of SWNT–substrate chemical interactions can reduce these problems, but they narrow the range of substrates and surfactants that can be used; these interactions can also have adverse effects on SWNT properties.

A controlled flocculation (cF) process provides an attractive alternative solution. This method involves actively driving SWNTs out of solution through the addition of liquids that are miscible with the suspending solvent and that also interact with the surfactant, in a way to disrupt its capacity to stabilize the SWNTs. When applied during the casting step, this cF process can yield, in a single step, films with *D* selected over a wide range.[78,79] For this process to produce uniform films of SWNTs without significant presence of bundles, the fluids must be confined close to the surface of a target substrate during mixing. This confinement may be accomplished in several different ways. In one case, methanol and aqueous suspensions of SWNTs are confined as a thin liquid film close to the surface of the receiving substrate by simultaneously introducing them onto a rapidly spinning substrate (Fig. 2a).[78] The associated shear flows help to confine the two liquids vertically and to mix them rapidly, favoring the formation of uniform coatings of individual or minimally bundled SWNTs (Fig. 2b). Shear forces associated with fluid flows can also lead to some degree of alignment, as illustrated in the atomic force microscopy (AFM) images in the inset of Figure 2b. In another approach, laminar flows in microfluidic channels provide the confinement.[79] The fluids flow side-by-side in a microchannel, and mix by diffusion only in a narrow region near the interface between the two liquids (Fig. 2c). SWNTs deposit in this region onto the substrate, forming a patterned film (Fig. 2d). This cF method can form films with *D*s that range from a small fraction of a monolayer to thick, multilayer coatings by simply increasing the duration of the procedure or the relative amounts of SWNT suspension and methanol, on a wide range of substrates with different surface chemistries, including low-energy surfaces, like those of polydimethylsiloxane (PDMS). This latter capability makes it possible to print the films in an additive, dry-transfer process simply by contacting a PDMS stamp coated with SWNTs to a higher-energy surface.[77–79]

Assembly techniques that form aligned arrays of SWNTs are important for applications in electronic devices because these arrangements avoid tube–tube contacts, which can limit charge transport through films.[80,81] This alignment can be induced by external forces, such as those associated with electric[82–87] or magnetic fields[88,89] and mechanical shear.[90–92] Alternating-current (ac) dielectrophoresis is notable[87] because it can be used not only to guide the deposition of partially aligned SWNTs to certain regions of a substrate but also to enrich the content of metallic tubes,[86] for applications such as transparent conductive coatings and photovoltaic devices.[93] The inset to Figure 2e shows a typical setup, where voltages applied to prepatterned microelectrodes create an electrical field. This field induces dipole moments in the SWNTs, especially in metallic tubes, due to their much larger polarizability, to attract the SWNTs and orient them along the field lines (Fig. 2e).[87] Alignment can also be achieved in other ways. In one example, convective flow of SWNTs to a liquid–solid–air contact line in a simple tilted-drop casting process creates nematic ordering with long-range alignment induced by narrow geometries chemically defined on surfaces.[94] Using a similar principle, arrays can be assembled using the

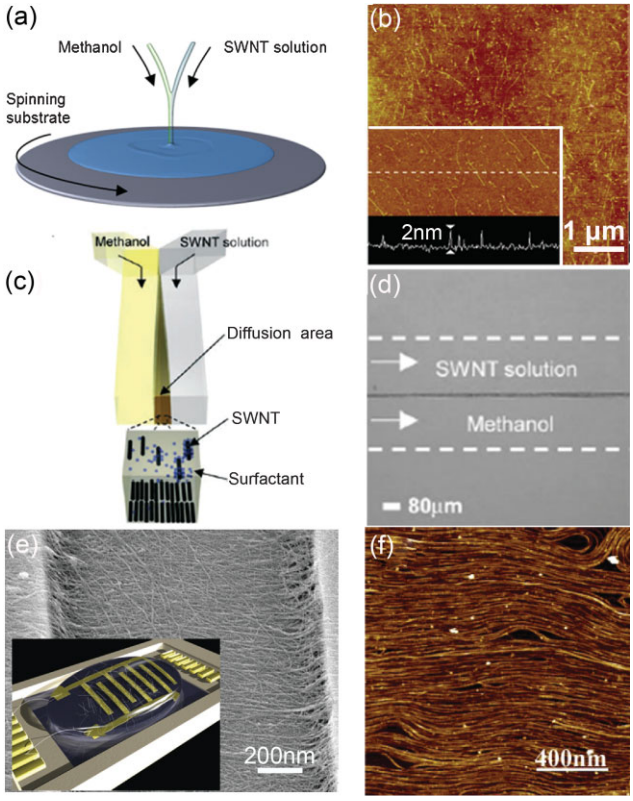

Figure 2. a) Schematic illustration of the deposition of uniform films of largely isolated, individual SWNTs in a cF process that involves mixing methanol and an aqueous suspension of SWNT on a rapidly spinning substrate. b) AFM image of an SWNT film deposited on plastic substrate in this manner. Inset: Magnified AFM image showing the radial alignment of SWNTs in a film deposited by cF on a spinning wafer. The bottom shows a line trace revealing the heights of individual SWNTs. Reproduced with permission from Ref. [78]. Copyright 2004 American Chemical Society. c) Schematic illustration of the deposition of films in line geometries by mixing methanol and a suspension of SWNTs in the interdiffusion region of a laminar-flow microfluidic cell. d) Optical image of a SWNT film in the geometry of a line (dark gray in the center of the image) deposited with a microfluidic cell, as illustrated in c). Reproduced with permission from Ref. [79]. Copyright 2006 Wiley-VCH. e) SEM image of an aligned SWNT film formed by ac dielectrophoresis. Reproduced with permission from Ref. [87]. Copyright 2006 Wiley-VCH. Inset: Schematic illustration of the experimental setup. An ac field applied through microelectrodes causes the deposition of aligned SWNTs, often with enhanced content of *m*-SWNTs. Reproduced with permission from Ref. [86] Copyright 2003 AAAS. f) AFM image of an aligned array of SWNTs assembled with a LB technique. Reproduced with permission from Ref. [95]. Copyright 2007 American Chemical Society.

Langmuir–Blodgett (LB) technique (Fig. 2f).[95] Films created in this manner can be transferred to various substrates (e.g., Si, glass, plastics) with the potential for repeated transfers to yield complex, multilayered structures.[77,96]

A main advantage of solution methods is that they can yield thin films directly at room temperature using SWNTs formed with bulk synthesis procedures, in a manner that is compatible with patterning techniques such as thermal, piezoelectric, or electrohydrodynamic jet printing.[97–99] A key disadvantage is that the SWNTs must be first dispersed into solution suspensions. This step often requires processes, such as high-power ultrasonication and strong-acid treatments, which degrade the electrical properties and reduce the average lengths of the tubes. In addition, the surfactant coatings represent unwanted organic contaminants for electronic devices. The development of new solubilization approaches might be needed to avoid these features.

2.2. Chemical Vapor Deposition (CVD) Growth

Films of SWNTs formed directly by CVD exhibit high levels of structural perfection, long average tube lengths, high purity, and relative absence of tube bundles compared to those derived from the techniques described in the previous section. The CVD method also provides excellent control over *D*, morphology, alignment, and position, to an extent that is unlikely to be possible by solution deposition. The value of *D* is important, due to its strong influence on electrical properties of the films. Several strategies in CVD can be used to control *D*. For example, the composition and flow rate of the feeding gas are important. With ethanol as the carbon feedstock, *D* significantly increases compared to the case of methane, possibly due to the ability of OH radicals to remove seeds of amorphous carbon from catalytic sites in the early stages of growth (comparing Fig. 3a and b).[100,101] Although some hydrogen is necessary to prevent the pyrolysis of carbon to form soot,[102] recent results suggest that the addition of water or oxygen can scavenge excess H radicals and thereby increase *D*.[103,104] The nature of the catalyst is also important. For example, catalysts of Fe/Co/Mo on silica supports[104–106] yield densities higher than those obtained from discrete iron nanoparticles, due to increased surface area, pore volume, and catalytic activity (comparing Fig. 3b and c). The concentration of the catalyst can also determine *D*. Other critical properties of the tubes, such as diameter distributions and, possibly, chiralities, can be influenced by the size[107–112] and composition of the catalyst.[113–116] Growth temperature, pressure, and time can also affect properties, such as average tube length.[117,118]

The CVD method also provides opportunities to control the alignment of the SWNTs. The driving force for alignment can arise from electrical fields,[119,120] laminar flow of feeding gas,[121–125] surface atomic steps,[126,127] as well as anisotropic interactions between SWNTs and single-crystalline substrates.[128–131] Electric fields ($>1\,V\,\mu m^{-1}$) can induce torques, which are sufficiently large to overcome random thermal motions, on growing SWNTs, even at the high-temperature growth conditions, thereby yielding field-aligned SWNTs (Fig. 3d).[119,120] In another approach, convective flow resulting from the temperature difference between the substrate and feeding gas can lift either catalyst nanoparticles[121,125] or SWNTs[123] from the surface of the substrate. In this lifted configuration, laminar flow can align the SWNTs in free space, in such a manner that they can fall back onto the substrate in their aligned state.[124] These methods lead to well aligned, millimeter-long nanotubes in a method that is relatively tolerant of debris or defects on the substrate. With multiple growth steps, complex

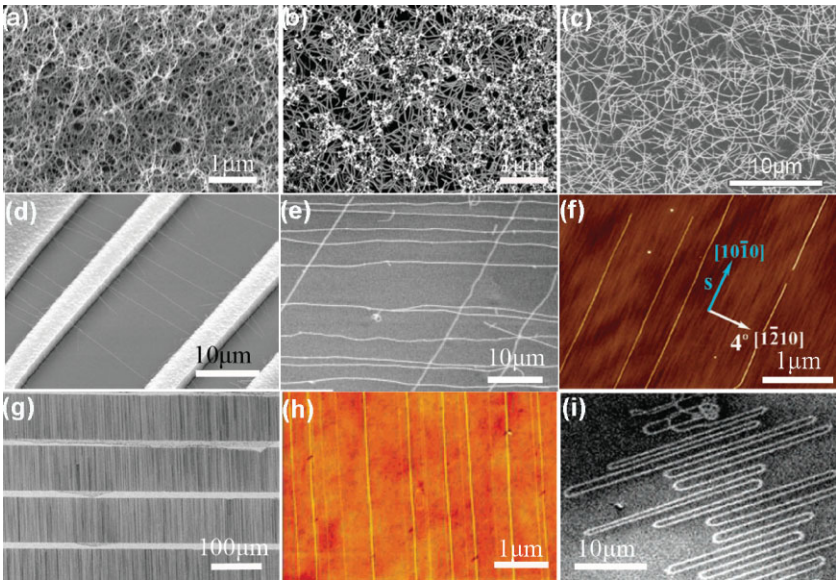

Figure 3. SEM images of SWNT films grown by CVD with a) ethanol and b) methane as the feeding gas, and Fe/Co/Mo catalysts on silica supports. c) SEM image of a SWNT film formed with methane feeding gas and ferritin catalysts deposited from a suspension in methanol. d) SEM image of an aligned array of SWNTs grown by CVD with an applied electric field between microelectrodes (white). Reproduced with permission from Ref. [120]. Copyright 2001 American Institute of Physics. e) Crossbar array of SWNTs formed by a two-step flow-alignment growth process. Reproduced with permission from Ref. [125]. Copyright 2003 Wiley-VCH. f) AFM image of an SWNT array grown on a miscut sapphire substrate. Reproduced with permission from Ref. [127]. Copyright 2005 American Chemical Society. g) Low-resolution SEM image of aligned arrays of SWNTs grown by CVD with methanol and Fe catalyst patterned into 10 μm wide stripes (bright horizontal lines) on quartz. h) AFM image of selected SWNTs in these arrays. i) Self-organized nanotube serpentines formed due to the combined alignment effects from the quartz substrate and gas flow. Reproduced with permission from Ref. [130]. Copyright 2007 American Chemical Society.

layouts, such as multilayer crossbar arrays, are possible (Fig. 3e).[125] Disadvantages include difficulty in achieving high *D* or perfectly linear shapes, due to thermal motions of the SWNTs and slight fluctuations in the gas-flow direction.

Interactions between SWNTs and atomic structures on single-crystalline substrates can enable arrays with nearly perfect alignment and linearity. For example, miscut c-plane sapphire substrates offer parallel, regularly spaced 2 Å high atomic steps[126] and 1.3 nm high faceted nanosteps after annealing;[127] both can serve as templates to guide nanotube growth through increased contact area for van der Waals interactions, uncompensated dipoles for electrostatic interactions, and improved wetting of catalyst nanoparticles due to capillarity (Fig. 3f). The lattice structure of some single-crystalline substrates, such as ST-cut single-crystal quartz and a-plane/r-plane sapphire, can yield arrays of nanotubes due to orientationally anisotropic interaction energies between the SWNTs and the substrates.[128,129] The degree of alignment depends on the surface quality and cleanliness and the underlying physics of the interactions. The highest levels of alignment and the highest levels of *D* can be achieved simultaneously, with catalysts patterned into small regions on quartz, such that the tubes grow primarily in regions of the substrate that are uncontaminated by unreacted catalyst particles.[132] Figure 3g shows scanning electron microscopy (SEM) images of such aligned SWNT films, grown from catalyst patterned into narrow stripes oriented perpendicular to the preferred growth direction on quartz. The images show excellent alignment and linearity in tubes with lengths of ~100 μm and in uniform densities over large areas (up to 2.5 cm × 8 cm, limited by the CVD chamber.) The tubes are nearly perfectly linear, with maximum deviations typically less than 5 nm, comparable to the resolution of the AFM (Fig. 3h). The tubes are also parallel to one another to better than 0.1 degree. The average *D* can be as high as 5–10 SWNT μm^{-1}, with peak values of 50 SWNT μm^{-1}.[130,131] Compared with others, this approach appears to be the most promising means to create SWNT arrays for demanding applications such as those in high-frequency electronics, where high *D*, degrees of alignment, and linear configurations with a complete absence of SWNT–SWNT overlap junctions are important. Advanced growth approaches that combine several alignment schemes enable complex configurations of SWNTs, including crossbar arrays,[133] perpendicular arrays,[134] and serpentines (Fig. 3i).[130,135]

Although not as convenient for large-area substrates as solution approaches, CVD methods are intrinsically scalable for realistic applications, as evidenced by their widespread use for other materials in various areas of electronics. Moreover, means to transfer high-quality CVD SWNT films from growth substrates to other substrates, including flexible plastic sheets, have been established recently, thereby expanding their applicability. The details of these transfer methods will be further discussed in Section 6.1.

2.3. Thin Films of Purified SWNTs

The ability to create collections of only semiconducting SWNTs (*s*-SWNTs) can be useful for nearly all applications of SWNTs, including those that use thin films (although, as described subsequently, it is *not* a requirement in this case). Enrichment can be achieved under certain conditions at the growth stage,[136,137] but approaches where *s*-SWNTs and metallic SWNTs (*m*-SWNTs) are separated after synthesis appear to offer the greatest level of control.[138] Such separation may arise from differences in i) electrical properties, ii) chemical properties, or iii) optical properties between *s*-SWNTs and *m*-SWNTs. The extent of separation is most commonly characterized through Raman/UV–vis spectroscopy or by direct electrical measurements.

Differences in electrical properties represent the most relevant features that distinguish *s*-SWNTs and *m*-SWNTs for applications

in electronics. The most direct way to exploit these differences in a separation scheme involves the operation of a TFT device that incorporates collections of tubes. Here, increasing the bias between the source/drain (S/D) electrodes while a gate field is applied to turn the *s*-SWNTs "off" leads to selective electrical breakdown of the *m*-SWNTs in aligned arrays of tubes, or the purely metallic percolation pathways in networks of tubes. This procedure, which was originally demonstrated with a FET constructed on an individual multiwalled tube,[139] can increase the on/off current ratio by up to 10^5 without significantly decreasing the on-state currents (I_{on}).[64,140–142] Difficulties in applying this approach to complex circuits, where independent electrical access to all transistors might not be feasible, limits its utility. Methods for wafer-scale implementation of this type of approach would be valuable.

A different class of strategy utilizes charged polymers, such as single-stranded deoxyribonucleic acid (DNA) and certain surfactants, to encapsulate SWNTs and suspend them into solutions.[143,144] Some of these polymers can induce image charges in *m*-SWNTs, which results in lower linear charge density and/or higher packing density of *m*-SWNT–polymer complexes compared with their *s*-SWNT counterparts.[145–148] Subsequent separation can be achieved through either ion-exchange chromatography or ultracentrifugation.[145,147,149–151] For ultracentrifugation, the tube diameter, electronic type, and length can also influence the buoyant density and the viscous drag,[147,152] respectively, thereby providing a route to separation according to diameter, electronic type, or length, depending on the nature of surfactants (Fig. 4a). Diameter control can be important for applications in electronics because the diameter influences the band gap, work function mobility, and mean free path for charge transport.[7] The length can influence the nature of charge transport through the networks, as described in detail in the following sections. These sorting procedures are especially effective for high-quality SWNTs synthesized by the laser-ablation method, and can be performed in multiple cycles to achieve degrees of separation sufficiently high to construct TFTs with on/off switching ratio above 10^4 even at relatively high *D* and short channel length (L_C, Fig. 4b).[147,153] Some other polymers with specific functional groups can selectively bind with *s*-SWNTs or *m*-SWNTs due to their structure and diameter differences, enriching certain types in the supernatant or on selectively functionalized surfaces.[154–156]

Differences in chemical reactivity can also be exploited for separation.[157–164] Experiments and calculations suggest that *m*-SWNTs are more chemically reactive than *s*-SWNTs, possibly because their finite density of states (DOS) near the Fermi level can stabilize charge-transfer complexes that form reaction intermediates.[165,166] Ideally, under certain conditions, only *m*-SWNTs will react with chemical reagents, rendering them insulating without altering the properties of *s*-SWNTs. For example, diazonium can react preferentially with *m*-SWNTs at optimized concentrations, as indicated by Raman spectroscopy (Fig. 4c).[165,167] The intensity of the disorder mode in *m*-SWNTs at ~1300 cm^{-1} increases upon reaction, which suggests an increase in sp^2 carbon. At the same time, the tangential mode at ~1590 cm^{-1} decreases and at ~169 cm^{-1} disappears, both of which are consistent with an increase in the level of structural defects. Much less pronounced changes occur for most *s*-SWNTs under the same conditions. Only with increased diazonium concentration, e.g., 10 μM for the conditions studied, does Raman spectroscopy indicate similar reactions with *s*-SWNTs. These observations are consistent with in situ electrical

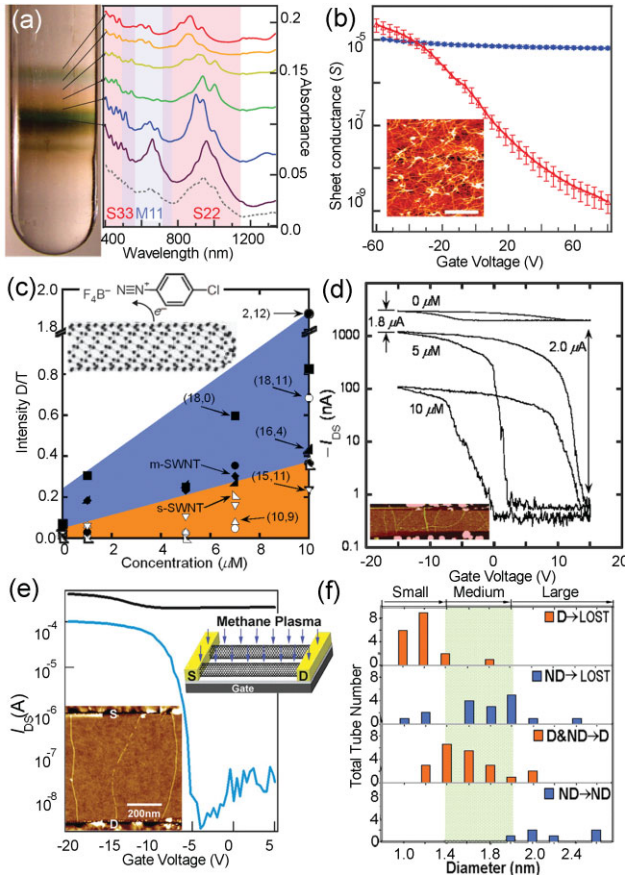

Figure 4. a) Optical image and absorbance spectra for SWNTs enriched by diameter and electronic type, via ultracentrifugation. The second- and third-order semiconducting and first-order metallic optical transitions are labeled as S22, S33, and M11, respectively. b) Transfer characteristics of SWNT TFTs made with enriched semiconducting (red) or metallic (blue) SWNTs. Inset: AFM image of an SWNT film used for a similar device (scale bar: 1 μm). Reproduced with permission from Ref. [147]. Copyright 2006 Nature Publishing Group. c) Ratios of the intensities of the disorder mode to tangential mode in Raman spectra (intensity *D*/*T*) of different SWNTs after functionalization, due to exposure to diazonium salt at various concentrations. Filled and open symbols refer to *m*-SWNTs and *s*-SWNTs, respectively. Each symbol corresponds to a specific tube with the indicated chiral index, assigned from the radial breathing mode. Inset: illustration of the selective reaction between *m*-SWNTs and diazonium salt. Reproduced with permission from Ref. [165]. Copyright 2003 AAAS. d) Transfer characteristics of an SWNT TFT before and after functionalization ($V_{DS} = -0.1$ V) plotted in logarithmic scale. Inset: AFM image of the channel region showing that most tubes directly span the S/D electrodes. Reproduced with permission from Ref. [167]. Copyright 2005 American Chemical Society. e) Transfer characteristic of an SWNT TFT before and after selective plasma etching, plotted in logarithmic scale. Upper inset: Schematic illustration. Lower inset: AFM image of part of a device channel region after plasma etching, showing one SWNT severely damaged. f) Diameter distribution of SWNTs with different responses toward plasma etching. (ND, nondepletable; D, depletable; LOST, electrically insulating.) Reproduced with permission from Ref. [168]. Copyright 2006, AAAS.

measurements on devices (Fig. 4d).[167] In particular, at moderate concentrations, device on-state (I_{on}) and off-state (I_{off}) currents decrease by similar amounts, consistent with selective elimination of conduction pathways through the *m*-SWNTs. The result is a sharp increase in the on/off ratio without significant reductions in the device mobility. Similar results are observed in gas-phase reactions with methane plasma.[168] Here, AFM shows that *m*-SWNTs are selectively etched into short segments by hydrocarbonation. The on/off ratios in devices increase by four orders of magnitude, as shown in Figure 4e. Both approaches are promising, but the reactivity also depends on SWNT diameter, which determines the radius of curvature and thus hybridization configurations of C–C bonding (Fig. 4f). As a result, the range of reaction variables (i.e., concentration, temperature, etc) that ensures selective reaction with *m*-SWNTs but not with *s*-SWNTs is small, especially for devices that use SWNTs with a wide distribution of diameters and chiralities. This delicate balance reduces the practical value of these methods. Other similar chemistries might be developed to circumvent this limitation.

As another route to separation, it might be possible to exploit the different band structures of *m*-SWNTs and *s*-SWNTs through their UV-vis-near-infrared (NIR) absorption spectra, as shown in Figure 4a. One can conceive, for example, of a light-induced ablation process[169] that could remove *m*-SWNTs and not *s*-SWNTs. In this manner, it might be possible to utilize a light source with appropriate wavelength and intensity to selectively eliminate *m*-SWNTs. Although some recent publications suggest such a capability, through indirect or direct means, additional work to optimize the approaches and to reveal the fundamental mechanisms might be required.[169–171]

In summary, although promising methods to separate solution suspensions of SWNTs are beginning to emerge, achieving simplicity and low-cost operation with an ability to remove all of the *m*-SWNTs without degrading the *s*-SWNTs remain important goals. Techniques capable of application directly to pristine CVD tubes on substrates would be extremely valuable, particularly for processing the sort of aligned configurations and high-quality SWNTs that are possible in this case. Progress made so far suggests that a reliable method may be available soon, perhaps by combining ideas from selective synthesis and post-synthesis sorting.[151]

3. Properties of SWNT Thin Films

The electrical properties of networks and arrays of SWNTs formed using the methods described in the previous sections are the basis for their application in electronics and sensors. In films that include many SWNT–SWNT junctions, the electrical transport involves percolation and flow of charge through many tubes when probed on length scales that are much larger than the average distance between junctions. The behavior, then, is controlled by the lengths of the SWNTs, their degree of alignment (i.e., density of SWNT–SWNT junctions), the distribution of electronic properties, and *D*. In films that involve perfectly aligned arrays of SWNTs, on the other hand, these percolation pathways are absent, and charge transport occurs directly through multiple tubes, each of which acts as an independent, parallel channel. The following summarizes experimental and theoretical studies of the films, and concludes with a description of some of their unique optical and mechanical properties.

3.1. Conducting Films of SWNTs

As synthesized, SWNT thin films contain roughly 1/3 *m*-SWNTs and 2/3 *s*-SWNTs. The high intrinsic conductivities of the *m*-SWNTs, together with the relatively long lengths that can be achieved, render the films, at sufficiently high *D*s, attractive as conducting layers, especially for applications requiring high frequency (~10 GHz) and high electrical field ($>10\,kV\,m^{-1}$), or those that benefit from low optical absorption or mechanical robustness.[172,173] Such films in random configurations, which are sometimes referred to as metallic carbon nanotube networks (*m*-CNNs) can achieve low sheet resistances, R_S, with superior mechanical/optical properties and the ability to be integrated onto a wide range of substrates.[76,77,106] Methods described in the preceding section can be used to form *m*-CNNs with selected *D*s and sheet conductances in cost-efficient ways to meet the requirements of different applications, such as transparent conductors for displays or touch screens.[69,76,106,174,175] The dependence of R_s on D can be approximated by standard percolation theory according to[69,176]

$$R_s = k(D - N_c)^{\alpha} L_S^{\beta} \quad (1)$$

where k is a fitting constant, N_c is the percolation threshold, L_S is average tube length, α is a parameter determined by the spatial arrangement of SWNTs in the film, and β is a parameter determined by the tube–tube junction resistance and SWNT conductivity. For an infinite 2D homogenous percolation network, N_c can be expressed as

$$L_s\sqrt{\pi N_c} = 4.236 \quad (2)$$

Experimental and theoretical analysis suggest that the van der Waals adhesive force between SWNTs leads to even lower percolation thresholds, by increasing the contact lengths between SWNTs.[177]

3.2. Semiconducting Films of SWNTs

SWNT thin films with moderate/low *D* or with enriched content of *s*-SWNTs can behave collectively as semiconducting networks (*s*-CNNs), for use in active electronic devices. This section describes experimental and theoretical studies of relationships between network properties and electrical characteristics, some features associated with the electrostatic coupling of such films to planar electrodes in transistors, the role of SWNT–metal contacts, and the use of chemical modifications to engineer the properties of such devices.

3.2.1. Percolation Modeling of SWNT Thin Films

Fundamental, predictive knowledge of the physics of transport through moderate/low *D* SWNT films is important to interpret and optimize the electrical performance when used as the semiconducting components of transistors. The classical percola-

tion theory outlined in Section 3.1 only addresses homogenous infinite networks. For applications in transistors, the electronic heterogeneity of the SWNTs, their anisotropic alignment, and the finite extent of the thin films make it necessary to develop nonlinear, finite-size percolation models, for predictive assessment of the properties.[178–181] The key geometrical parameters for such modeling, including average tube length (or stick length, L_S), L_C, and width of the transistor channel (W) or of the strips defined in the networks (W_S, as described subsequently), are depicted in Figure 5a. In the linear response region of device operation, drift-diffusion theory can be used to describe transport within individual sticks, according to $J = q\mu n d\varphi/ds$, where J is current density, q is carrier charge, μ is mobility, n is carrier density, φ is electropotential, and s is length along the tube. When combined with the current continuity equation, $dJ/ds = 0$, this expression gives the nondimensional potential φ_i along each tube i according to $d^2\varphi_i/ds^2 - c_{ij}(\varphi_i - \varphi_j) = 0$. Here, $c_{ij} = G_0/G_1$ is the dimensionless charge-transfer coefficient between tubes i and j.[180] The network is assumed to contain metallic and semiconducting tubes at a ratio of 1:2. I_{on} and I_{off} correspond to the sum of fluxes through all sticks and through just the purely metallic transport pathways, respectively. The finite W or W_S is incorporated by use of reflecting boundary conditions at the edges of the network.[182] For transport in completely random networks, this approach can successfully predict the scaling behavior with W, W_S (Fig. 6b), L_C, and D, based on models that randomly populate a 2D grid with sticks of fixed length (L_S) and random orientation (θ).[66,182] For partially aligned networks, the degree of alignment, as defined in terms of an anisotropy parameter, R, where $R = L_{//}/L_{\perp} = \sum_{i=1}^{N} |L_{S,i} \cos\theta_i| \Big/ \sum_{i=1}^{N} |L_{S,i} \sin\theta_i|$, can be described with a probability density function to control how sticks populate the 2D grid. Both L_S and R are typically determined through analysis of experimental images of the networks. For a wide range of L_S and R values, as shown in Fig. 5b, where L_S changes from 5 to 40 μm and R changes from 2.9 to 21.4, the experimental data (symbols) and simulation results (lines) agree well.[183] Results obtained in a similar study also show that for partially aligned SWNTs, when $L_C > L_S$, where no single SWNT can bridge the S/D electrodes directly, the transconductance is maximized for an optimum R, which lies between a completely random network and perfectly aligned array to achieve a balance between reducing SWNT–SWNT junctions and increasing conductance pathways formed by misaligned SWNTs. If, on the other hand, $L_C < L_S$, then there is no need for the formation of pathways composed of multinanotubes, and the transconductance is always improved with increasing degree of alignment.[184]

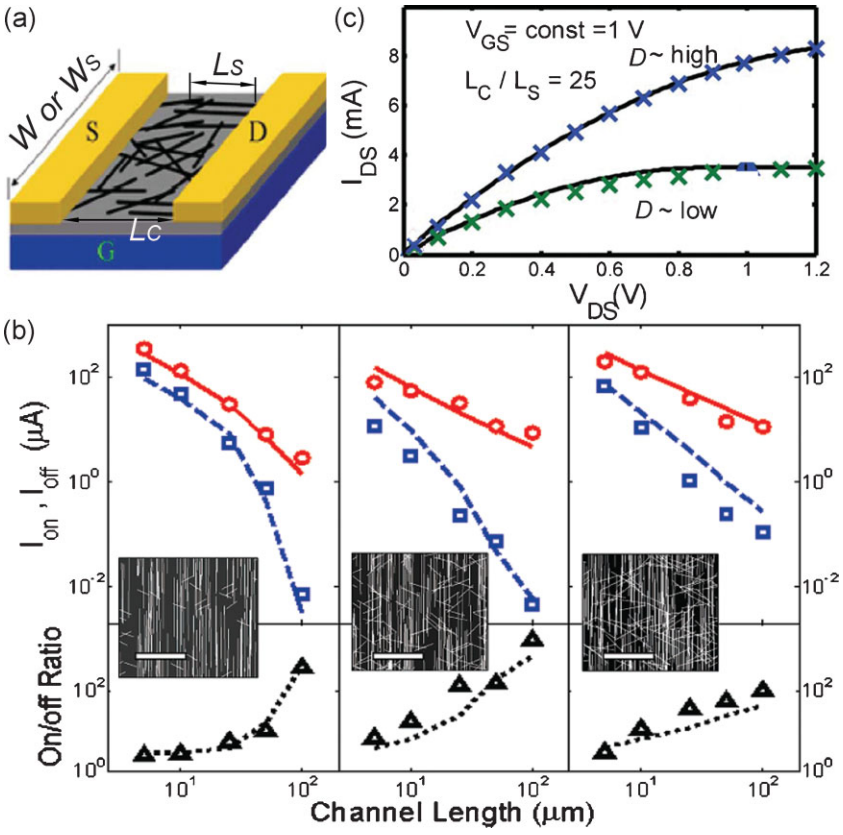

Figure 5. a) Schematic illustration of a model system for heterogeneous percolative simulation. SWNTs are represented as sticks with finite lengths, corresponding to the average tube length (L_S). These sticks populate the device channel region, defined by a width (representing either channel width, W, or strip width, W_S) and channel length (L_C), at a density D. b) Measured (symbols) and computed (lines) properties of SWNT TFTs. From left to right, these films range from well-aligned, low-coverage to partially aligned, high-coverage cases. The plots show I_{on}, I_{off}, and on/off ratio for aligned (left), partially aligned (middle), and dense partially aligned (right) networks. Insets: images of the simulated networks, where the scale bar has a length of 10 μm. Reproduced with permission from Ref. [183]. Copyright 2007 American Chemical Society. c) Measured (symbols) and simulated (lines) $I_{DS} - V_{DS}$ characteristic of SWNT TFTs with high (blue) and low (green) densities, respectively. Reproduced with permission from Ref. [185]. Copyright 2007 IEEE.

In the saturation region of device operation, the conductance along the channel is no longer a constant, making it necessary to solve self-consistently both the Poisson equation and drift-diffusion equation. Surprisingly, such modeling shows that the conductance exponent term for the saturation regime is exactly the same as that in the linear regime. The behavior of the devices can, therefore, be described by the following universal formula:

$$I_D = \frac{A}{L_S}\left(\frac{L_S}{L_C}\right)^{m\left(DL_S^2\right)}\left[(V_{GS} - V_T)V_{DS} - \gamma V_{DS}^2\right] \qquad (3)$$

where A is proportional to the gate capacitance, the diameter distribution of the SWNTs, and the resistances at SWNT–SWNT

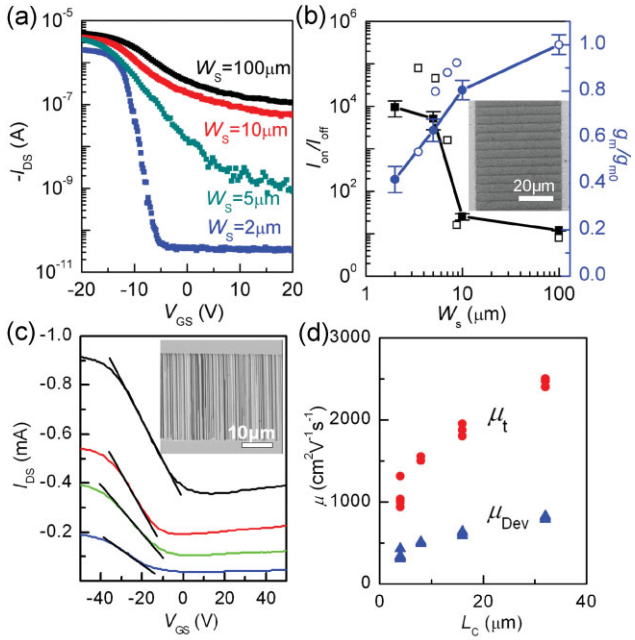

Figure 6. a) Transfer characteristics of TFTs with L_C of 100 μm and W of 100 μm, based on SWNT random networks cut into strips with W_S of 100, 10, 5, and 2 μm, from top to bottom, along the electron-transport direction, in logarithmic scale (V_{DS}: −0.2 V). b) The measured (filled) and simulated (open) influence of W_S on the on/off ratio (I_{on}/I_{off}) and normalized device transconductance (g_m/g_{m0}, where "0" represents the state without strips) for SWNT devices shown in a). Inset: SEM image of the channel region of such a device. Reproduced with permission from Ref. [66]. Copyright 2008 Nature Publishing Group. c) Transfer characteristics of TFTs based on aligned arrays of SWNTs with L_C of 5, 10, 25, 50 μm, and W of 200 μm (V_{DS}: −0.5 V). The straight lines serve as visual guides to indicate the slopes used to extract the linear region g_m. Inset: SEM image of the channel region of such a device. d) Mobilities (μ) calculated using parallel plate model for capacitance (μ_{DEV}) and per-tube mobilities calculated considering only the capacitance coupling between *s*-SWNTs and planar gate electrode (μ_t) as a function of L_C. Reproduced with permission from Ref. [64]. Copyright 2007 Nature Publishing Group.

junctions, γ is an independent geometrical parameter typically ~0.5, and m is a universal exponent of stick percolation systems. With a given A, V_T, and γ, this equation describes the characteristics of transistors with arbitrary L_S, L_C, and D in both linear and saturation regions, as shown in Fig. 5c.[185] The good agreement of these theoretical results with experiments suggests that heterogeneous percolation models can accurately describe the physics of transport in SWNT thin films with any layout, in both linear and saturation regimes. These observations enable quantitative interpretation of the transport behavior of SWNT thin films and also help to guide optimization of their layout design and properties, as described in the following section.[184,186]

3.2.2. Relationship Between Film Layout and Properties

In addition to length, orientation distribution, and other aspects, the spatial arrangement of SWNTs strongly influences the overall electrical properties of the films. A pristine, as-synthesized SWNT random network is electrically isotropic. Lithographic patterning and etching procedures provide a route to engineering the layouts of such networks, to advantage. For example, cutting a network into narrow strips (width, Ws) oriented along the overall transport direction (Fig. 6b inset) limits the lateral crosstalk between SWNTs, such that the percolation thresholds rise with decreasing W_S. Such increases in threshold affect I_{off} more than I_{on}, because the *m*-SWNTs are less abundant than *s*-SWNTs, and because the I_{off} in the network device arises from pathways that involve only *m*-SWNTs. As a result, etched strips in the network can lead to orders of magnitude decreases in I_{off} by significantly reducing the possibility of purely metallic pathways. At the same time, their adverse effects on the I_{on} variability and effective mobility, both of which are strongly determined by *s*-SWNTs (Fig. 6), can be comparatively minor when implemented in optimized geometries.[66] The role of these strips on the electrical properties of SWNT thin films can also be quantified through percolation modeling discussed in the previous section (Fig. 6b).[182] This type of engineering of the layouts of SWNT networks offers opportunities to achieve high on/off ratio without steps to enrich the population of *s*-SWNTs or to remove the *m*-SWNTs.

The collective properties of random networks or partially aligned SWNT thin films in the limit of $L_C > L_S$ are influenced not only by the properties of the SWNTs themselves, but also by the finite resistance and electrostatic screening at the SWNT–SWNT junctions.[80,81] Perfectly aligned arrays of SWNT assembled using the guided growth methods described in Section 2.2, with $L_C < L_S$, can avoid these SWNT–SWNT contacts altogether, thereby enabling certain electrical characteristics of the films to approach intrinsic properties of the individual SWNTs.[64,130,184] Figure 6c depicts a series of transfer characteristics of transistors that use aligned arrays. The effective mobilities (μ_{DEV}), extracted from devices with long L_C (e.g., > 25 μm) where the effect of parasitic contact resistances are small, approach 1000 cm^2 Vs^{-1}, which is a 10-fold improvement over that of values reported for random networks. The per tube mobilities (μ_t), calculated using the capacitance only of the *s*-SWNTs in the arrays, as described below, can exceed 2000 cm^2 Vs^{-1}, which is only slightly lower than the diameter averaged intrinsic mobilities (~3000 cm^2 Vs^{-1}, Fig. 6d) evaluated from sets of devices constructed on single tubes.[64] These attractive properties, at a reproducible, scalable level in thin-film devices, allow this class of material to be considered for high-performance electronic systems, as described further in Section 7.

3.2.3. Capacitance Coupling of SWNT Thin Films

The electrostatic capacitance coupling between a planar electrode and a SWNT thin film, which is generally in a sub-monolayer format for optimal use as a semiconducting material, is critically important for transistor operation and for estimating the performance limits of SWNT TFTs. This coupling can be much different than that of traditional thin-film type materials, depending on D and on the separation between the planar gate electrode and the film (d), due to the SWNT film's limited surface coverage and stick topology.[187,188] A simple model system, consisting of a parallel array of equally spaced SWNTs, can provide a semiquantitative understanding of the gate capacitance

coupling in SWNT TFTs that use films with some degree of misalignment and/or nonuniform spacings (Fig. 7a).[189] Finite-element simulation reveals that the fringing fields and electrostatic screening between neighboring SWNTs can lead to electrical field distributions, and therefore capacitance coupling to a gate electrode that deviate significantly from that of a parallel-plate capacitor (Fig. 7b). An analytical expression of gate capacitance (C_i), which assumes that the charge distributes symmetrically around the nanotube (consistent with a single sub-band quantum limit), can be obtained for the case of nanotubes that are fully embedded in a material with the same dielectric constant (ε) as the gate dielectric,

$$C_i = \left(\frac{2}{\varepsilon}\log\frac{\Lambda_0}{R_T}\frac{\sin\pi 2d/\Lambda_0}{\pi} + C_Q^{-1}\right)^{-1}\Lambda_0^{-1} \qquad (4)$$

where Λ_0 is the average distance between neighboring tubes; R_T is the tube radius, and C_Q^{-1} is quantum capacitance. In most regimes, this equation yields results similar to direct, finite-element simulation (Fig. 7c). The validity of these models has been confirmed, qualitatively and semiquantitatively, through experiments on SWNT TFTs with a range of dielectric thicknesses as well as direct capacitance–voltage measurements.[66,189] This knowledge is critical in comparing the effective mobilities of SWNT thin-film devices with different *D*s and *d*s, and in obtaining accurate transient state analysis of such devices and circuits that incorporate them.

3.2.4. Electrical Contacts Between SWNT Films and Metallic Electrodes

For transistors built on individual SWNTs, two distinct types of behaviors have been reported. The first involves field-effect modulation of apparent device resistance through changes in the properties only of the contacts, and not the channel.[190–192] Devices of this type are often referred to as Schottky-barrier (SB) transistors. The second type of reported operation is due to a more conventional mechanism, in which the field effect modulates the properties of the channel. Here, the contacts contribute a simple, Ohmic, and field-independent resistance.[7,193–195] These two dramatically different operational-mode cases can result, at least in part, from differences in the SWNTs (e.g., diameters, densities of defects, etc), in the metals for the contacts, and in extrinsic features associated with the details of device processing. The ability to form large collections of SWNT TFTs with good uniformity in properties allows standard transmission-line model (TLM) analysis of their behavior. The first, and simplest, observation that emerges from an analysis of random network devices with moderate *D*s and L_Cs significantly larger than the average distance between tube junctions is that the device mobilities, as evaluated without specifically including the effects of the contacts, are only weakly dependent on L_C. This outcome is consistent with a small role of contacts in the device operation (Fig. 8a).[142,196–198] A more detailed study, using standard TLM procedures,[199] involves first determining the resistance of semiconducting pathways (R_{sem}) from the overall device resistance, by assuming that R_{sem} (the resistance associated with the semiconducting pathways) and R_{met} (the resistance associated with the metallic pathways, as determined from I_{off}) are connected in parallel. Plotting this quantity (R_{sem}) as a function of L_C at a range of gate-source voltages (V_{GS}) provides key insights. In particular, the *y*-intercepts and inverse slopes of linear fits to such data yield the contact resistance and the channel sheet conductance, respectively, at each V_{GS}. The results reveal that V_{GS} significantly modulates the conductance of SWNT films in a manner that is quantitatively consistent with silicon-device models. Furthermore, the contact resistance is negligible compared with the channel resistance for L_C larger than ~2 μm, for the example here. The "intrinsic" mobility (μ_{int}) can be calculated by subtracting the effects of contact resistance; the results are almost identical to values extracted directly from transfer characteristics of individual devices (Fig. 8b inset).

By contrast, for TFTs built with aligned arrays of SWNTs, the effects of contacts can be prominent, due mainly to the lowered channel resistances in this case compared to that of the random network devices. These effects can be seen most simply through the strong dependence of the mobilities extracted from transfer characteristics, ignoring the effects of contacts, on L_C (Fig. 8a). In particular, the mobilities increase with increasing L_Cs, and approach μ_{int} at long L_Cs, where the channel resistance is sufficiently large to dominate the device behavior (Fig. 8c inset).[64] Full TLM analysis shows that even in aligned-array devices, the total device resistance changes mainly due to modulation of the channel sheet conductance by V_{GS}; the properties of the contacts change by a comparably small amount (i.e., by an amount less than experimental uncertainty for these data) with V_{GS} (Fig. 8c). The contact resistance pertube, as evaluated from the *y*-intercept and the estimated number of *s*-SWNTs involved in transport, is ~30 kΩ,[64] close to the value, ca. ~21 kΩ, extracted from measuring transistors built on individual tubes.[7] Chemical-doping approaches demonstrated for single-tube devices, or new metallic materials for S/D

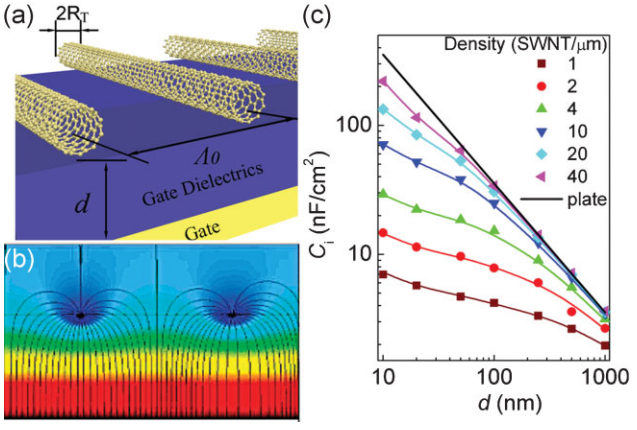

Figure 7. a) Schematic illustration of a model system used to calculate the capacitance coupling between an array of SWNTs and a planar electrode. Λ_0: average distance between neighboring tubes; R_T: tube radius; *d*: dielectric thickness. b) Simulation of the electropotential distribution of this system evaluated with the finite-element method (FEM). The black lines correspond to the field lines. c) Capacitances (C_i) for capacitors formed with SWNT arrays with different densities, SiO_2 dielectric layers with different *d*s, and planar electrodes, computed with FEM (symbols) and an analytical expression (lines). Reproduced with permission from Ref. [189]. Copyright 2007 American Institute of Physics.

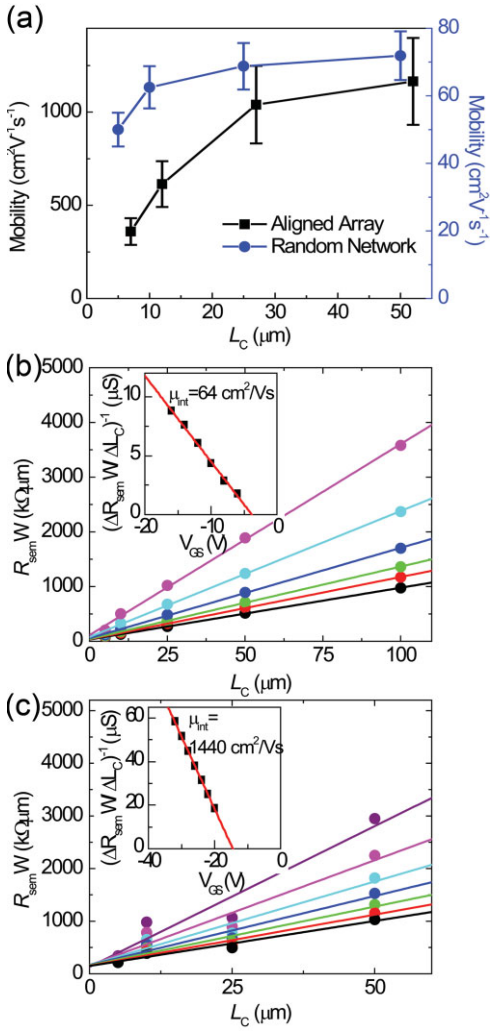

Figure 8. a) Linear region device mobilities, extracted from transfer characteristics and capacitances calculated using a rigorous model, of SWNT TFTs based on aligned arrays ($D \sim 5$ SWNT μm^{-1}, left axis, square) and random networks ($D \sim 6$ SWNT μm^{-2}, right axis, circle). Width-normalized resistance of semiconducting responses of TFTs ($R_{sem}W$) based on b) SWNT random networks and c) aligned SWNT arrays as a function of L_C at different V_{GS} (in frame b, V_{GS} changes from −6 to −16 V in step of 2 V from top to bottom. In frame c, V_{GS} changes from −20 to −32 V in step of 2 V from top to bottom). The solid lines represent linear fits. Although all fitted lines show similar intercepts, this outcome is just a coincidence of the linear regression fitting process. The relative standard errors for the fitted intercepts are between 40 and 200%. Insets: Plots of the sheet conductance $(\Delta R_{sem}W/\Delta L_C)^{-1}$ associated with the semiconducting responses, determined from the reciprocal of the slopes of the linear fitting in the main frames, as a function of V_{GS}, giving the "intrinsic" device mobilities (μ_{int}) after subtracting influences from contact resistances.

electrodes, may help to reduce the contact resistance.[200,201] In all cases, the work functions and chemistries of the contact metals can have important effects on performance and polarity of SWNT TFTs. High-work-function metals, such as palladium/gold, provide efficient contacts for p-channel devices; with decreasing work function, ambipolar and n-channel behavior can be observed. Similar results have been reported for devices constructed on individual tubes.[192,202,203]

3.2.5. Chemical Modifications of Transport

Transport in SWNTs is known to be sensitive to their surrounding environment, due to the high surface to volume ratios of the tubes.[204] SWNT TFTs that use as-grown or as-deposited nanotube networks/arrays typically exhibit unipolar p-channel behavior when built with high work function metals for S/D contacts and exposed to oxygen, at least partly due to the presence of SBs at the contacts.[190,205] Such devices can be converted to air-stable n-channel or ambipolar modes when they are passivated with inorganic dielectrics.[206,207] The mechanism behind this process could involve elimination of oxygen molecules that otherwise collect on the sidewalls of SWNTs and/or SWNT–metal contact in open air.[205,208–210] In this view, removal of absorbed oxygen renders s-SWNTs as intrinsic (i.e., undoped) semiconductors[205,210,211] and/or reduces the SBs for electron conduction, such that both electrons and holes can be injected from S/D electrodes[190,212] (Fig. 9a). Charge-transfer doping with amine-containing molecules/polymers provides a convenient means to achieve similar control, as initially demonstrated in single-tube devices.[213,214] This strategy works for SWNT TFTs with conventional gate dielectrics as well as those that use polymer electrolytes.[142,196–198,215] In particular, uniformly coating the channel region with low molecular weight polyethyleneimine (PEI) leads to unipolar n-channel operation in as-fabricated p-channel devices (Fig. 9b). These behaviors are thought to arise from changes in the electrical properties of nanotubes themselves, due to the polymer coatings.[197,216] The effective device mobilities of n-channel devices that result from this process are generally somewhat inferior to those of their p-channel counterparts, possibly because of incomplete coating/interaction of the PEI with the tubes or residual electron withdrawing species adsorbed onto the devices prior to coating. Control of device polarity by simple application of dielectric/polymer coatings is effective for random networks, aligned arrays, or anything in between. This capability represents an advantage of SWNT TFTs compared to organic TFTs, where completely different chemistries for the semiconducting materials are typically used for p-channel, n-channel, and ambipolar devices.[217–219]

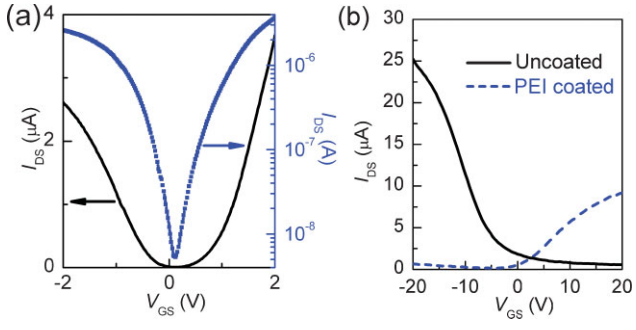

Figure 9. Transfer characteristics of a) ambipolar, b) unipolar p-channel, and unipolar n-channel SWNT TFTs achieved with a) dielectric passivation or b) polymer charge-transfer doping.

3.3. Optical and Mechanical Properties

Although the band gaps of SWNTs are relatively small, films of the type described in the preceding sections can be relatively transparent to visible light for several reasons. First, because of their small diameter and high aspect ratio, SWNTs exhibit low, polarization-dependent optical absorption cross-sections.[220] Second, SWNTs have low plasma cut-off frequencies.[76] Third, their high intrinsic mobilities and conductivities enable films with even relatively low coverage to provide good electrical properties. Compared to traditional transparent conductive/semiconducting oxides such as indium-doped tin oxide (ITO) or zinc oxide (ZnO), such SWNT films can provide higher performance and with a potential for lower cost. They are, therefore, under exploration for use in transparent passive and active electronic devices, as discussed in detail in Section 4. SWNT thin films also offer excellent mechanical properties due in part to the intrinsic mechanical properties of the SWNTs, that is, high elastic moduli and fracture stresses.[20,221,222] Experiments suggest that even under exerted high strain levels (~5%), the electrical properties of SWNT thin films only vary within 15%.[20,223] These features make SWNT films attractive for applications that require high degrees of mechanical bending, such as flexible or conformable electronic systems, which will be further discussed in Section 6.

4. Transparent Electronics Based on Carbon-Nanotube Thin Films

Invisible electronic materials are of special value for many military and consumer applications, such as antistatic coatings, flat panel displays, photovoltaic devices, and certain security components.[224] Metal oxides, for example, ZnO and ITO, are the most widely used materials in such applications. They have, however, several limitations: i) they are costly and ITO is becoming increasingly expensive due to a predicted shortage of indium; ii) they have facture strains less than 1%,[225] resulting in limited mechanical robustness; iii) their deposition requires vacuum procedures and, often, elevated temperatures; iv) semiconductor films typically demonstrate modest mobilities (up to ~20 $cm^2\ Vs^{-1}$).[226,227] By contrast, SWNT thin films, which can be produced in large quantities by arc-discharge and/or CVD methods and then deposited and patterned with cost-efficient solution processes or printing procedures (see Section 2.1 and 6.1), offer outstanding electrical, optical, and mechanical properties, as discussed in Section 3. As a result, such materials have emerged as promising candidates for transparent electronics.[173,228] In this section, we describe the development of transparent conductive SWNT films, where the aim is to replace ITO/ZnO for certain applications. We then introduce some examples of the integration of transparent SWNT thin films into functional active electronic and optoelectronic devices.

4.1. Transparent Conductive Films of Carbon Nanotubes

Although the idea of utilizing SWNT films as conductive materials is simple, the overall properties depend in complex ways on many parameters including average tube length, tube diameter, deposition method, abundance of *m*-SWNTs, and adventitious doping from the ambient.[76,229] For conductive films, long SWNTs, to minimize the role of SWNT–SWNT junctions in transport, with relatively large diameters, to minimize the band gap of *s*-SWNTs, are preferred.[175,230] Ideally, the deposition method should allow assembly of uniform films at high throughput on any substrate, with accurate control of *D*. Several of the techniques described previously have attractive capabilities, most notably the cF and vacuum-filtration methods.[69,76,78] These approaches can yield uniform coatings over large areas. Figure 10a shows such a film 50 nm thick covering a 4 inch diameter wafer, with sheet resistance $< 100\,\Omega\ sq^{-1}$ and transmittance greater than 70% over the visible range, both comparable to properties of ITO films with similar thickness. The conductance can be further reduced by doping *s*-SWNTs with strong acid/oxygen or by hybridizing with gold nanoparticles.[231–234] Films made with *m*-SWNTs collected by ultracen-

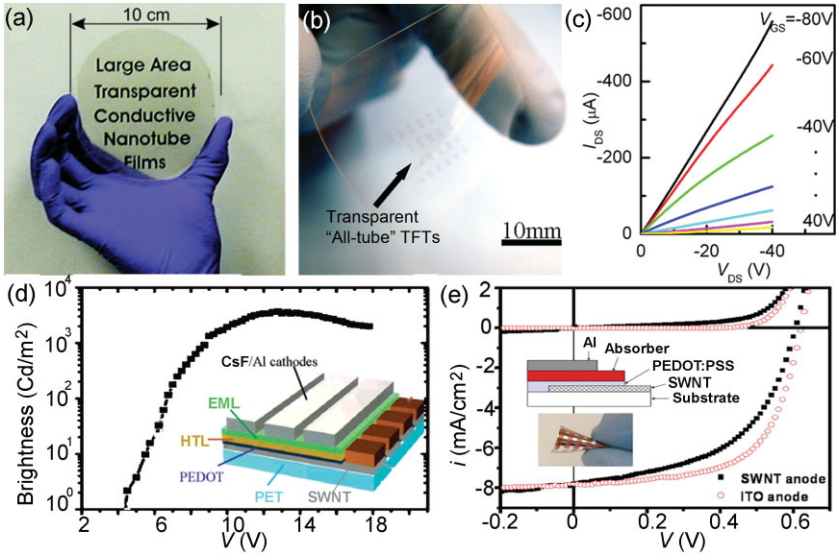

Figure 10. a) Optical image of a transparent, conductive SWNT film on a sapphire substrate. Reproduced with permission from Ref. [76]. Copyright 2004 AAAS. b) Optical image of an array of "all-tube" flexible transparent TFTs (TTFTs) on a plastic substrate. The arrow indicates the S/D structures, which are faintly visible as arrays of gray squares in the center of this image. c) $I_{DS} - V_{DS}$ characteristic of a SWNT TTFT (V_{GS} changed from −80 to 40 V in steps of 20 V). Reproduced with permission from Ref. [106]. Copyright 2006 Wiley-VCH. d) Brightness versus voltage for an OLED that uses a SWNT thin film as the anode. Reproduced with permission from Ref. [250]. Copyright 2006 American Chemical Society. Inset: Schematic illustration of the device layout of OLED. HTL, hole-transport layer; EML, emission layer. Reproduced with permission from Ref. [230]. Copyright 2006 American Chemical Society. e) Current density (*i*) versus voltage for organic solar cells that use ITO or SWNT thin films (black square) as the anode. Inset: Schematic and optical image of flexible organic solar cell using SWNT thin film as electrodes on PET substrate. Reproduced with permission from Ref. [251]. Copyright 2006 American Institute of Physics.

trifugation have sheet resistances as much as 10 times smaller than those of films formed with identical procedures but using unsorted SWNTs.[235] Also, films made with *m*-SWNTs that have a narrow diameter distribution demonstrate a colored appearance, thus opening the possibility for use in conductive optical filters.[235]

4.2. Applications in Active Transparent Electronics and Optoelectronics

Transparent conducting and semiconducting films have been demonstrated in various active-device structures, ranging from TFTs to optoelectronic devices and microelectromechanical systems/nanoelectromechanical systems (MEMS/NEMS).[106,236–241] The ability to form transparent TFTs is interesting because it suggests a path to invisible circuits.[242] Such devices can be realized by combining, for example, either SWNT-film electrodes (i.e., high *D*) and transparent organic semiconductors, or metal oxide electrodes and semiconducting SWNT films (i.e., moderate or low *D*).[106,243,244] Here, we highlight an approach to flexible transparent transistors that uses SWNT films for all of the current-carrying layers.[106] Figure 10b shows an optical image of an array of this type of ''all-tube'' transparent TFTs. Such devices can be formed through sequential transfer printing of CVD nanotube networks with different densities onto a plastic substrate. High-*D* films form the S/D and gate electrodes, while moderate-*D* films form the semiconductor. The optical transmittance, even for the most opaque S/D regions, is above 75%, comparable to some of the best transparent transistors based on oxides.[227,245] These devices demonstrate attractive electrical properties, with effective mobilities of $\sim 30\,cm^2\,Vs^{-1}$, comparable to or somewhat larger than those of typical amorphous semiconducting oxides, $<20\,cm^2\,Vs^{-1}$. (Fig. 10c).[227,245] These performance attributes suggest potential use in applications that are more advanced than switching transistors in active-matrix liquid-crystal displays. When combined with mechanically robust elastomeric dielectrics, the devices can withstand tensile strains up to 3.5% without degradation. Beyond this limit, the dielectrics fail, but the SWNT films remain conductive/semiconducting.

Transparent conductive SWNT films are of particular interest for optoelectronic devices based on organic semiconductors, such as organic light-emitting diodes (OLEDs) and organic photovoltaic devices (OPVs), as a replacement for ITO to realize low-cost roll-to-roll manufacturing.[246] In addition, SWNTs can provide excellent contacts to organic semiconductors[243] without the disadvantages of ITO, such as diffusion of oxygen into organic layers, absorption in the blue region, and poor mechanical robustness/chemical stability.[225,247,248] Since SWNT films exhibit relatively high work functions ($\sim$4.9 eV),[249] they can serve as electrodes for hole-injection/extraction in OLEDs/OPVs. For optimum results, a poly(3,4-ethylenedioxythiophene)/poly (styrene sulfonate) (PDOT/PSS) coating, which offers higher work function ($\sim$5.2 eV), is often applied to the SWNT layer, to improve device efficiency and to planarize the SWNTs (Fig. 10 d and e inset). Luminescence above 3000 cd m^{-2} and turn-on voltages around 5.0 V have been reported in flexible OLEDs; power efficiencies up to 2.5%, comparable to that of devices with ITO electrodes, have been achieved in flexible OPVs, all using SWNT thin films as the anode electrodes (Fig. 10d and e).[250–252] Experiments also show that replacing ITO with SWNT films as electrodes does not alter device lifetimes.[250]

5. SWNT Thin Films for Sensing

The electronic properties of SWNTs, which consist exclusively of surface atoms, are very sensitive to adsorbents.[204,205] Changes can be electrically evaluated in resistor, transistor, or capacitor structures. In this manner, it is possible to incorporate SWNTs as sensing elements for various molecules of interest, from toxic chemical vapors to bio-macromolecules.[253–255] Compared with individual nanotubes, SWNT thin films, where a large number of tubes are exposed to analytes simultaneously, not only improve the signal-to-noise ratio and thus the detection limit,[256] but they can also be used conveniently to build large numbers of identical devices, as discussed previously. In this section, we summarize various device-structures/sensing strategies specially engineered for SWNT thin films in gas or biomolecular sensors.

5.1. Gas Sensors

SWNT gas sensors respond to the surface coverage of analytes (P/P_0, where P is the partial pressure and P_0 is equilibrium pressure, respectively), unlike conventional gas sensors, which respond to their concentration (P).[257,258] As a result, they can offer very high, ca. $\sim$part per billion (ppb) level, detection limits for low vapor pressure analytes such as chemical warfare agents and explosives, which cannot be detected by conventional gas sensors for which such concentrations are insufficient to load the active materials.[257–262] The simplest sensor is a chem-resistor, which involves electrical contacts at two ends of a SWNT thin film, as represented by the flow cell shown in Figure 11a inset.[260] Gas molecules adsorb onto the surfaces of the SWNTs, especially at defect points.[263] Experiment and calculation suggest that charge transfer between adsorbed molecules and the SWNT valence band changes the number of mobile charge carriers, and thus the apparent resistance.[208,264] Molecules with strong electron-donating or withdrawing capabilities lead to large changes in resistance. Dimethyl methylphosphonate (DMMP), a simulant for the nerve agent sarin, can be detected at ppb levels due to its high electron-donating properties (Fig. 11a).[260] The recovery of resistance can be slow, however, due to high desorption energies, thus limiting the dynamic range/reversibility. One solution to this problem is to form the SWNT sensor in a TFT geometry. By application of a suitable gate voltage, the resistance can be nearly completely reset to its initial value, possibly due to the action of repulsive Coulomb forces between adsorbents and the gate-induced charge (Fig. 11b).[260]

Besides monitoring variations in the conductance of SWNT thin films, sensing can be accomplished by measuring the changes in capacitance between the film and a planar electrode in a chem-capacitor structure (Fig. 11c inset).[257] The capacitance response comes from changes in i) quantum capacitance of SWNTs, due to the shift of Fermi level as a result of charge transfer doping associated with adsorbed molecules, and ii) geometrical capacitance, due to the change of dielectric environment closely surrounding SWNTs, as a result of both

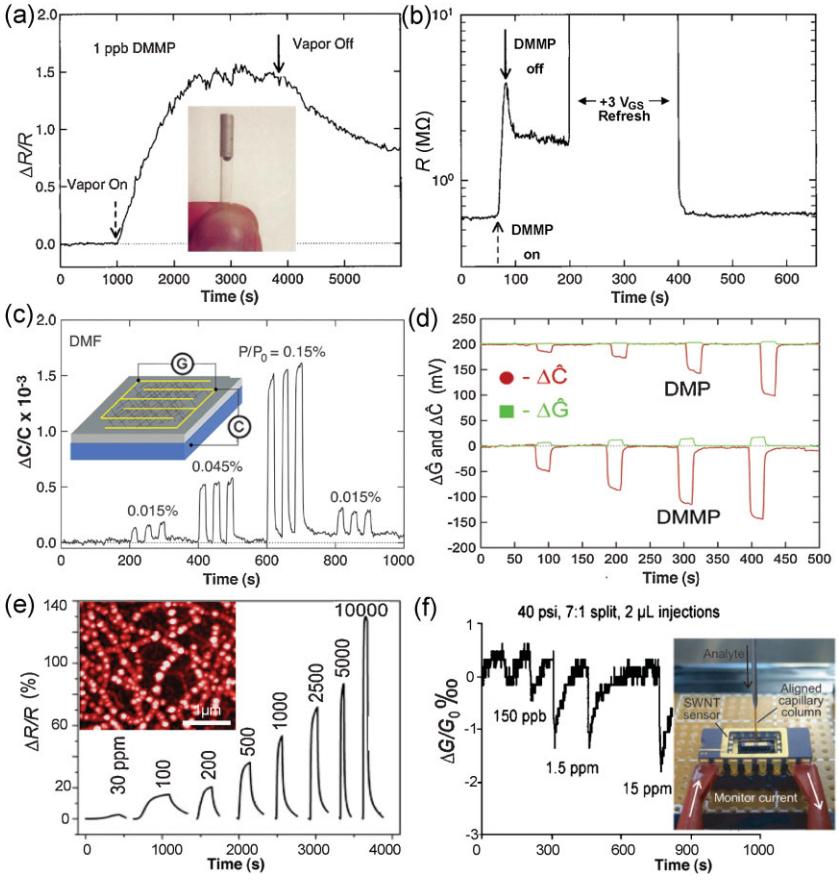

Figure 11. a) Relative change in resistance ($\Delta R/R$) versus time for a SWNT chem-resistor loaded in a flow cell exposed to 1 ppb DMMP. Inset: Optical image of a SWNT flow cell chem-resistor sensor. b) Resistance (R) versus time for a SWNT chem-transistor in response to exposure to DMMP and subsequent bias voltage applied to the gate. Reproduced with permission from Ref. [260]. Copyright 2003 American Institute of Physics. c) Relative change in capacitance ($\Delta C/C$) versus time for a SWNT chem-capacitor exposed to doses of *N*,*N*-dimethylformamide (DMF) at varying concentrations noted in the figure. Reproduced with permission from Ref. [257]. Copyright 2005 AAAS. d) Normalized change in capacitance ($\Delta\hat{C}$, red) and conductance ($\Delta\hat{G}$, green) versus time for a SWNT sensor exposed to doses of DMMP and dimethyl phosphite (DMP) at varying concentrations. Reproduced with permission from Ref. [265]. Copyright 2005 American Chemical Society. e) $\Delta R/R$ versus time for a SWNT chem-resistor decorated with Pd nanoparticles exposed to hydrogen at varying concentrations (in the unit of ppm) noted in the figure. Reproduced with permission from Ref. [267]. Copyright 2007 Wiley-VCH. Inset: AFM image of Pd nanoparticles deposited on a random network of SWNTs via electroplating. Reproduced with permission from Ref. [268]. Copyright 2007 American Institute of Physics. f) Relative change of conductance ($\Delta G/G_0$) versus time of a SWNT sensor exposed to DMMP pulses through an integrated μ-GC column. Inset: Optical image of the integrated μ-GC system with SWNT gas sensor as detector. Reproduced with permission from Ref. [274].

electric-field alignment of dipole moments and field-induced polarizations of adsorbed molecules.[257] Because an ac field is utilized in capacitance measurements, molecules are forced to undergo continuous adsorption–desorption processes. This feature leads to rapid and reversible behavior (Fig. 11c).[257] Unlike conductance, the capacitance responses do not require strong interactions with the absorbed molecules or direct charge transfer, the latter of which is likely to happen only at some finite "active" sites, for example, defect points. The result is an ability to detect over a large range of concentrations.[258] The different mechanisms for conductance and capacitance responses lead to different responses to analyte molecules with similar structures (Fig. 11d).[265] The ratio of the change in conductance to the change in capacitance can be used as a characteristic signature to distinguish different chemical vapors.

A major disadvantage of SWNT gas sensors is lack of specificity. One way to solve this problem is to functionalize SWNTs with specific receptors for targeted analytes. For instance, decorating SWNTs with either evaporated or electroplated palladium nanoparticles (Fig. 11e inset) leads to the formation of a SWNT chem-resistor specific for hydrogen detection.[266–268] When exposed to hydrogen, the reversible formation of electron-rich palladium hydride hinders hole transport in p-doped *s*-SWNTs, and thus leads to higher resistance.[269] Due to the availability of abundant active sites in SWNT thin films, these sensors can respond linearly over a wide concentration range, an obvious advantage over previous results from individual-tube devices (Fig. 11e).[267] A major source of interference for this sensor is oxygen, which also reacts with Pd.[269] Additional chemoselective coatings may help to solve this problem.[258,270] Similar strategies have also been developed for specific detection of H_2S, CH_4, and CO_2.[271–273] Another approach is to circumvent this issue entirely by integrating SWNT gas sensors into microgas chromatography (μ-GC) systems (Fig. 11f).[274]

5.2. Biosensors

Since the diameters and carrier densities of SWNTs are comparable to the sizes and surface-charge densities of bio-macromolecules, SWNTs can serve as ultrasensitive transducers in biosensors based on chem-resistor or transistor structures.[40,275,276] Biomolecules, such as DNAs and proteins, can nonspecifically bind to the surfaces of SWNTs, due to hydrophobic interactions, π–π stacking interactions,[143] and possibly amino-affinity of SWNTs to alter the conductance of SWNT thin films.[277] In this way, the SWNTs themselves can function as labels for efficient label-free detection (Fig. 12a and b).[278,279] Furthermore, single-strand DNAs bound to SWNTs can serve as probes for their complementary strands, to distinguish, for example, between mutant and wild-type alleles (Fig. 12c).[278,279] Generally, there are two mechanisms for biomolecules to influence the electronic properties of SWNTs: i) electrostatic gating or doping of SWNTs, and ii) modulation of the SB between SWNTs and contact electrodes.[280] Recent experiments in which only contact or channel regions of SWNT transistors were exposed to DNA solutions suggest that although both mechan-

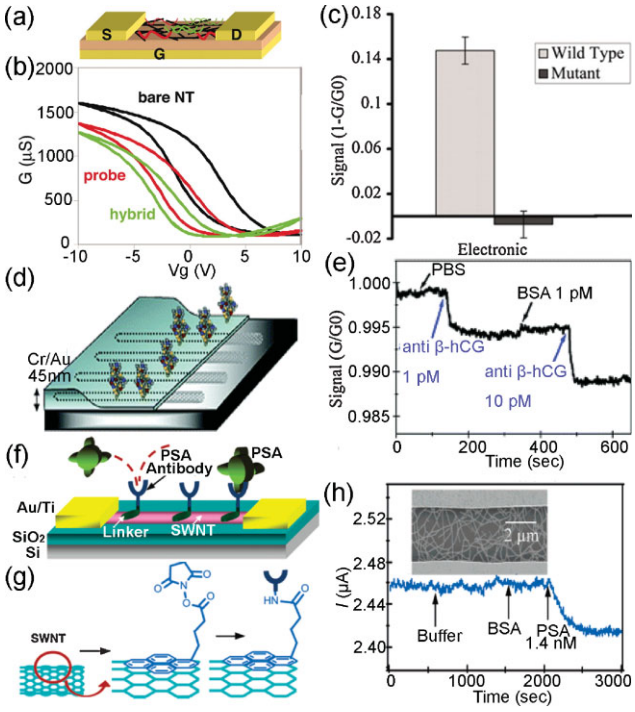

Figure 12. a) Schematic illustration of label-free detection of DNA using SWNT TFTs. b) Transfer characteristics of SWNT TFTs before (bare NT), and after incubation with 12-mer DNA probes (probe), as well as after incubation with the complementary DNA target (hybrid). c) Relative change in conductance ($1 - G/G_0$) for SWNT TFTs incubated with probe DNAs in response to the complementary (wild type) or single basepair mismatched (mutant) single-strand target DNA. Reproduced with permission from Ref. [278]. Copyright 2006 American Academy of Science. d) Schematic illustration of highly sensitive detection of biomolecules utilizing large-area Schottky contacts. e) Relative change of conductance (G/G_0) versus time for SWNT chem-resistor capable of specific detection utilizing antigen–antibody interaction of human chorionic gonadotropin (hCG) and mouse antibody (β-hCG). PBS, phosphate-buffered saline; BSA, bovine serum albumin. Reproduced with permission from Ref. [283]. Copyright 2006 American Chemical Society. f) Schematic illustration of noncovalent functionalized SWNTs for detecting prostate-specific antigen (PSA). g) Schematic illustration of the reaction sequence to functionalize SWNTs with anti-PSA monoclonal antibody (PSA-AB). h) Change in current versus time for a PSA-AB-functionalized SWNT thin-film chem-resistor exposed to buffer, BSA, and PSA. Inset: SEM image of SWNT thin film as the active layer. Reproduced with permission from Ref. [286]. Copyright 2005 American Chemical Society.

isms contribute to DNA sensing, contact modulation can be more significant.[281,282] The dominant role of contact modulation is also supported by measurements of transfer characteristics of SWNT TFTs, where both decreases of p-branch and increases of n-branch conductance were observed for DNA-functionalized devices (Fig. 12b).[278] The sensitivity of SWNT biosensors can therefore be improved by engineering the electrode profile to maximize the thin-metal contact area with SWNTs (Fig. 12d).[283] The detection limit can be increased by over 100 times to achieve picomolar- or even femtomolar-level detection limits in this manner.[283,284] Selective detection by use of antigen–antibody interactions can also be achieved in this structure, by first coating the device with antigens by nonspecific adsorption and then masking the remaining active sites with a surfactant. After these treatments, only addition of the corresponding antibody induces changes in conductance, without any response to other interfering proteins (Fig. 12e).[283]

A more generalized and reliable approach to achieve specific detection involves direct chemical functionalization of the SWNTs. Noncovalent approaches are generally preferred as they do not degrade the intrinsic electrical properties of the SWNTs.[285] Figure 12f and g schematically illustrate the use of a bifunctional small-molecule linker that binds with SWNTs through π–π stacking interactions and with an antibody through covalent bonding.[286] In this system, only the introduction of a specific antigen can change the conductance, presumably due to electrostatic gating effects (Fig. 12h). Other nanotube functionalization agents, such as polymers and dextrans,[287,288] and other specific biointeractions, such as enzyme–substrate interactions and aptamer–substrate interactions,[253,289–291] can also be utilized.

6. Application of SWNT Thin Films in Flexible, Conformable, and Stretchable Electronic Systems

Electronic devices that can be formed on mechanically flexible substrates have recently attracted considerable attention owing partly to the proliferation of handheld, portable consumer electronics and the attractive features that flexibility would bring to such devices.[67,292] In addition, many next-generation military and industrial radio-frequency (RF) surveillance systems and others benefit from flexible and large-area layouts. Currently, amorphous Si (a-Si), low-temperature polycrystalline silicon, and organic semiconductors represent the most widely explored materials for the semiconductor components of these systems.[293,294] Due to their modest electrical properties, applications that require substantial computational, control, or communication functions cannot be addressed. The combination of attractive electrical, mechanical, and optical properties of SWNT thin films renders them interesting candidates. Replacing organic semiconductors and a-Si in these flexible/stretchable systems or in *macroelectronic* devices, instead of competing with wafer-scale Si microelectronics, might represent the most realistic short/medium-term application goal.[67,142,292,295] In this section, we first discuss methods to integrate high-quality SWNT thin films on plastic substrates, with a focus on dry transfer printing techniques. We then describe several classes of SWNT TFTs, emphasizing device layouts and optimization, followed by circuit level demonstrations. Finally, we introduce recently developed classes of stretchable devices that use SWNT thin films on elastomer substrates.

6.1. Film Formation on Flexible Substrates

Although solution deposition methods are naturally compatible with plastic substrates, the films formed in this way generally have electrical properties that are significantly worse than those of films formed by CVD, at least in part due to their shorter average tube lengths, residual surfactant coatings, and structural defects induced by solubilization processes. Most CVD procedures for synthesizing SWNTs require, on the other hand, high tempera-

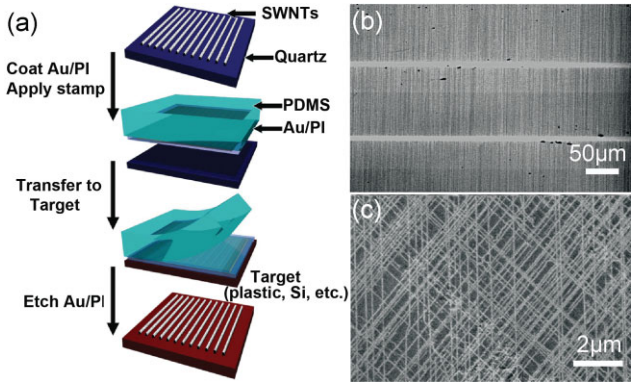

Figure 13. a) Schematic illustration of a process that uses polyimide (PI) and a gold (Au) film to transfer CVD-grown nanotubes (in this case, aligned arrays of SWNTs grown on quartz) to other substrates. SEM images of b) aligned SWNT arrays transferred from a single-crystal quartz growth substrate to a plastic substrate and c) triple crossbar arrays of SWNTs formed by three consecutive transfer processes. Reproduced with permission from Ref. [96]. Copyright 2007 American Chemical Society.

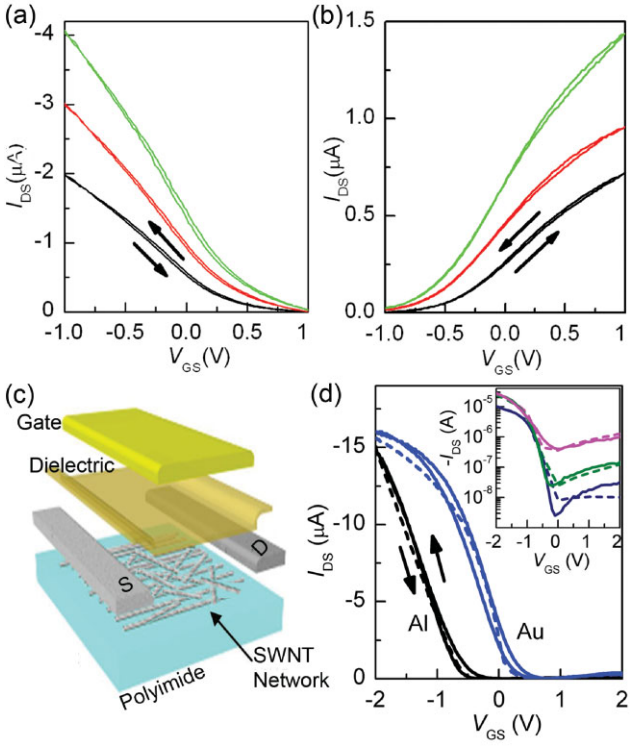

Figure 14. Transfer characteristics of SWNT TFTs on plastic substrates coated by bilayer nano-dielectrics, with L_Cs, from top to bottom, of 50 μm (green), 75 μm (red), 100 μm (black), a) before and b) after uniformly coating the channel region with PEI (V_{DS}: −0.2 V). Reproduced with permission from Ref. [198]. Copyright 2006 Wiley-VCH. c) Schematic illustration of a top-gate SWNT TFT on a plastic substrate. d) Transfer characteristics of top-gate SWNT TFTs with high k HfO_2 dielectric and high work function (Au, blue) and low work function (Al, black) gate electrodes. Inset: transfer characteristics of the SWNT with Al gate plotted on a logarithmic scale, with $V_{DS} = -0.5$ V (navy), −2 V (green), −5 V (magenta). Dashed lines are SPICE simulation results. Reproduced with permission from Ref. [66]. Copyright 2008 Nature Publishing Group.

tures (generally above 800 °C for thermal CVD and 450 °C for certain plasma-enhanced methods). Such conditions prevent the direct growth of nanotubes on plastic and other potentially interesting materials.[296] Although microwave methods may allow tubes to be grown directly on plastic, further development is required to improve tube quality.[297] Transfer printing techniques avoid these challenges by separating the high-temperature CVD synthesis from target substrates with limited thermal stability. One such technique uses PDMS stamps to remove SWNT films from a growth substrate such as SiO_2/Si after HF etching of the oxide.[223] This method is simple and has very high efficiency. The values of D evaluated on the receiving substrate are almost the same as those on the growth substrate. Related methods that use "carrier" films, which adhere strongly to the SWNTs and may serve as plastic substrates for subsequent device/circuit fabrication, can transfer tubes directly without undercut etching (Fig. 13a).[66,96,298–300] Such approaches can be used, for example, to transfer aligned nanotubes grown on quartz (Fig. 13b).[96,300] In both cases, a metal film, which is subsequently removed by wet-etching after transfer, can be applied on top of SWNT films to bind them together during the printing processes. Multiple transfer steps enable further control of D and tube layouts (Fig. 13c).[96]

6.2. Mechanically Flexible SWNT Thin-Film Transistors

Conventional microfabrication techniques or printing approaches can be applied to SWNT films on plastic to form devices and circuits.[197] The gate dielectrics are important components of SWNT TFTs. High capacitances for low-voltage and hysteresis-free operation, together with low leakage current densities for power efficiency are desirable. Deposition methods

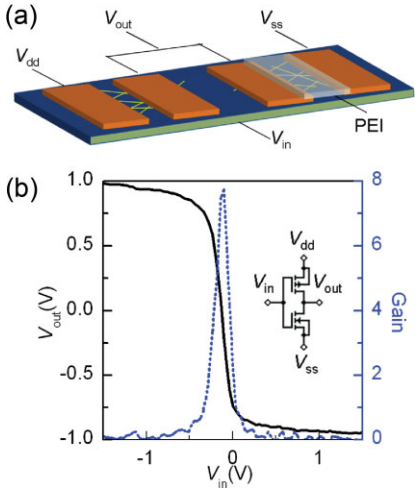

Figure 15. a) Schematic illustration and b) static transfer characteristics of a CMOS inverter formed with a pair of back-gated SWNT TFTs that use films of random networks of SWNTs and HfO_2/epoxy bilayer gate dielectrics. The n-channel TFT is coated with PEI. The inset of b) provides the corresponding circuit diagram. V_{dd}, common power supply; V_{in}, input voltage; V_{out}, output voltage; V_{ss}, common ground. Reproduced with permission from Ref. [198]. Copyright 2006 Wiley-VCH.

that are compatible with plastic substrates can also be important, depending on the application. Certain classes of 3D-crosslinked organic multilayers (~16 nm) formed through room-temperature self-assembly processes are attractive, due to the large capacitances (~170 nF cm^{-2}), excellent insulating properties (leakage current densities less than 10^{-9} A cm^{-2}) and smooth surface morphologies.[215,301] A different approach utilizes inorganic oxides (2–5 nm) formed by atomic layer deposition (ALD), with spin-cast crosslinked epoxies (~10 nm) on top to serve as adhesive layers for transfer printing, if necessary.[198] Such bilayer nano-dielectrics, similar to organic multilayers, offer high capacitance (up to ~330 nF cm^{-2}) as well as low leakage current density, interface charge density, interface state density, and dissipation factors. These high-capacitance dielectrics also greatly reduce the subthreshold swing (S) of SWNT TFTs, which enables operation at voltages even lower than those that would be inferred from the differences in capacitance. Therefore, hysteresis for both p-channel and n-channel devices built on bilayer nano-dielectrics or organic multilayers is much smaller than that of devices on more widely explored thick oxide or polymer dielectrics, possibly due to a reduction in the electrical fields near the SWNTs as result of lower operating voltage and fewer traps in dielectrics (Fig. 14a and b).[198,215,302,303]

Devices with such dielectrics can incorporate a bottom-gate structure, where a continuous conductive film, for example, ITO deposited on polyethylene terephthalate (PET) substrate, serves as a gate electrode.[198,223] This layout is easy to fabricate and is useful for evaluating the electronic properties of the devices, although it is not immediately suitable for circuit integration. There are two approaches to avoid this limitation. One is to use a patterned bottom-gate structure.[304] The advantage of this approach is that the nanotubes are exposed, thereby enabling their electronic properties to be further tuned with chemical modification techniques discussed in Section 3.2.5. When exposed to oxygen from the air, for example, the devices demonstrate unipolar p-channel behavior (Fig. 14a). Another approach is to deposit gate dielectrics on top of SWNTs for a top-gate device structure (Fig. 14c).[66] High k dielectrics can be deposited by ALD, for example, on CVD tubes transferred to a polyimide substrate. Such designs with random-network SWNT thin films offer good device properties, that is, mobilities ~ 70 cm^2 Vs^{-1}, subthreshold slopes ~200 mV dec^{-1}, operating voltages less than 4 V, transconductances as high as 0.12 μS μm^{-1} and on/off ratios $>10^3$ enabled by the striping scheme discussed in Section 3.2.2 (Fig. 14d).[66] Furthermore, because high-capacitance gate dielectrics reduce the relative contribution of voltage across the dielectric to the threshold voltage (V_T), V_T can be controlled using gate metals with different work functions.[63,305] For example, replacing Au with Al as the gate metal shifts V_T by −(0.6–0.8) V, thereby changing the device operation from depletion mode to enhancement mode. The behaviors of these SWNT TFTs can be described with standard models for silicon device technologies, for example, SPICE (simulation program for integrated circuits emphasis) models, thereby allowing the use of existing sophisticated computer-aided design platforms developed for silicon integrated circuits (ICs) (Fig. 14d).[66] A disadvantage of the top-gate device structure is that SWNTs are passivated, and thus isolated from external dopants, such as oxygen or polymers. Therefore, these transistors often exhibit some level of ambipolar behavior, which limits the on/off ratios at high S/D bias conditions (Fig. 14d inset). Small-molecule doping techniques similar to those demonstrated in single SWNT devices might be useful.[200] As discussed in the following section, even without such approaches, top-gate transistors can meet requirements for certain ICs.

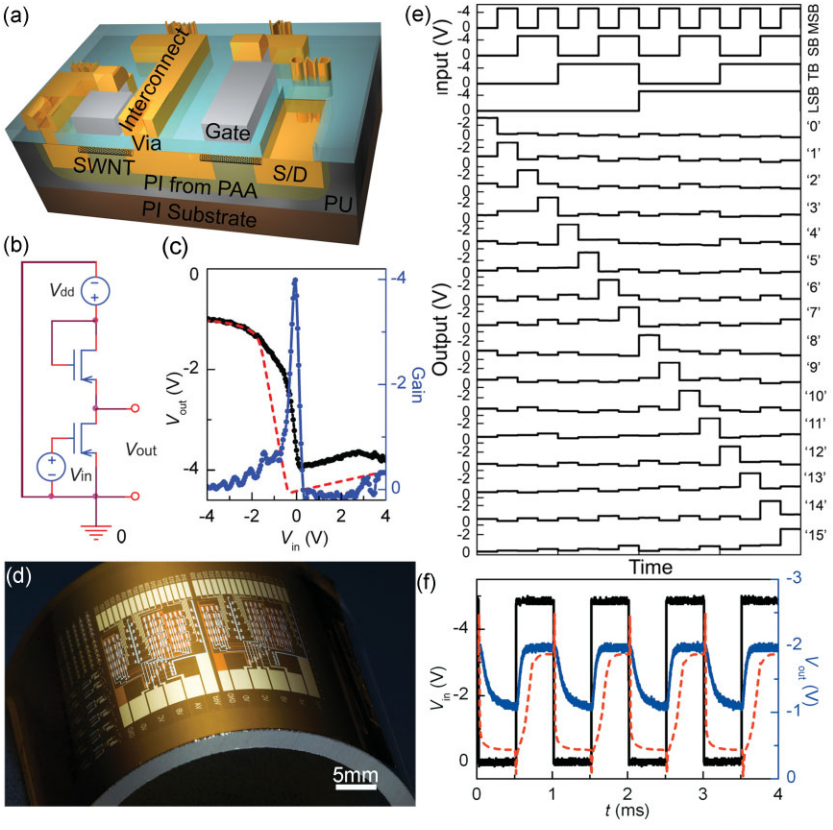

Figure 16. a) Schematic view, b) circuit diagram, and c) static transfer characteristics of an inverter composed of two p-channel SWNT TFTs on a PI substrate. PU, polyurethane; PAA, polyamic acid. In c), the dashed line represents a circuit simulation result. d) Optical image of a flexible SWNT integrated circuit chip bonded to a curved surface. e) Input–output characteristics of a four-bit decoder composed of 88 SWNT TFTs. In descending order, the first four traces are inputs, labeled as most significant bit (MSB), second bit (SB), third bit (TB), and least significant bit (LSB) on the right-hand side; the remaining traces, labeled "0" to "15", show the output voltages of the sixteen outputs. f) Measured (blue) and simulated (red) dynamic response of one output line under a square-wave input pulse (black) at a clock frequency of 1 kHz. Reproduced with permission from Ref. [66]. Copyright 2008 Nature Publishing group.

6.3. Flexible Integrated Circuits

Despite numerous achievements in optimizing various aspects of isolated SWNT TFTs, these devices are only of practical value when integrated into circuits. Since the polarity of SWNTs can be controlled by charge-transfer doping methods, as discussed in Section 3.2.5, a CMOS type inverter, which represents an important element in digital circuits, can be constructed by connecting a p-channel and an n-channel bottom-gate devices, doped by oxygen and polymers, respectively (Fig. 15a).[197,198,215,306] With high-capacitance gate dielectrics to enhance the transconductance and *S*, voltage gains approaching ten can be achieved, which is comparable to single-tube inverters based on local bottom-gated devices (Fig. 15b).[61,198] Similar circuits, such as CMOS NAND gates, have also been recently demonstrated.[306]

For more complex structures/functions, top-gate devices facilitate multilayer interconnects, and more importantly, computer-aided platforms to assist circuit design.[66] Figure 16a and b show a schematic layout and circuit diagram for a p-channel MOS (PMOS) inverter, the building block for PMOS-type logic circuits, fabricated on polyimide substrates with two separately addressable SWNT TFTs. The static transfer characteristics can be successfully predicted by simulations (Fig. 16c). The voltage gain is much larger than unity, and can thus be used to drive subsequent logic gates without losing logic integrity. Further integration yields SWNT-based digital circuits, composed of other logic gates and decoders, incorporating up to 88 transistors, which represents the largest SWNT circuit achieved to date (Fig. 16d). This circuit can successfully decode a binary-encoded input of four data bits into 16 individual data output lines, where one output is enabled, depending on whether the encoded value corresponds to the data line number (Fig. 16e). Due to the high mobility of the SWNT thin films, these decoder circuits can successfully operate in the kilohertz regime, even with critical dimensions (~100 μm) that are sufficiently coarse to be patterned by techniques such as screen printing (Fig. 16f).[307–309] This attribute is important for their potential applications in low-cost, printed electronics.

6.4. SWNT Thin Films in Stretchable Devices

Foldable and stretchable electronic systems have recently emerged into an interesting area of research.[310–313] The ultimate goal is to overcome form-factor limitations associated with systems that only offer flexibility (i.e., ability to wrap cylinders and cones), to enable applications such as wearable personal-health monitoring systems and electronic eye-type imagers on hemispherical substrates.[314,315] SWNTs, due to their excellent mechanical/electrical properties and sensitive electromechanical responses, are promising for such systems.[316,317] Simply loading a SWNT random network onto an elastomeric substrate affords a two-terminal stretchable resistor with the ability to accommodate strains greater than 20% (Fig. 17a).[318] Such strain leads to deformation of individual SWNTs in the network (Fig. 17b), thereby changing their electronic properties reversibly, due to changes either in band gaps and/or SWNT–SWNT contacts.[317,318] This property can be utilized to construct strain sensors with piezoresistance gauge factors (GF), defined as resistance modulation per strain, comparable with those of conventional metal-strain gauges (ca. GF 1–5, Fig. 17c). Alternative designs involve aligned arrays of SWNTs in sinusoidal "wavy" layouts, formed through nonlinear buckling processes (Fig. 17d).[20] Applied strains lead to reversible deformation of these buckling patterns (Fig. 17e) and changes in the electrical properties (Fig. 17f). Further improvement of GF in these devices to achieve performance comparable to those of gauges built with individual SWNT (GF as high as 1000),[317,319] and forming more complex multifunctional devices that can combine the active, sensory and structural capabilities of SWNTs, appear to represent promising future-research directions.

7. SWNT Thin-Film Radio-Frequency Analog Electronics

The combination of high intrinsic mobility (~10^4 cm^2 Vs^{-1}), small capacitance (~100 aF μm^{-1}), and nanometer-thick body channels

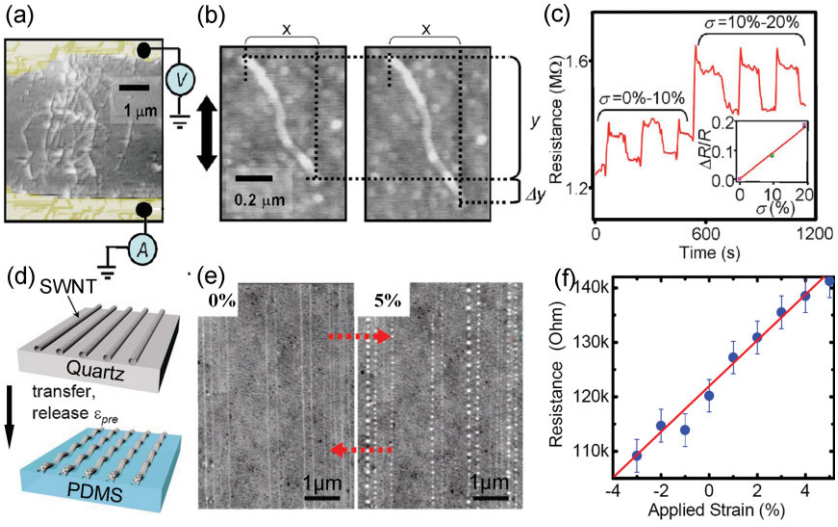

Figure 17. a) AFM image of a SWNT film loaded onto an elastomer substrate. Conductance was measured between two contact electrodes on upper and lower ends. b) AFM image shows the elongation of an individual SWNT in the film under external stress. c) The resistance change of a SWNT thin film to repetitive application of 0–10% strain and then 10–20% strain. Inset: the normalized resistance ($\Delta R/R$) change as a function of external strain (σ) of the device. The GF is ~1. Reproduced with permission from Ref. [318]. Copyright 2006 American Institute of Physics. d) Schematic illustration of the formation of "wavy" SWNTs by transfer of aligned arrays of SWNTs grown on a single-crystalline quartz substrate to a uniaxially strained PDMS elastomer substrate followed by release of the prestrain (ε_{pre}). e) AFM image of aligned arrays of SWNTs transferred to elastomer substrate with $\varepsilon_{pre} = 0$ before and after applying 5% compressive strain. f) Change of resistance of an array of wavy tubes as a function of applied strain. The GF is ~4. Reproduced with permission from Ref. [20]. Copyright 2008 American Chemical Society.

make SWNTs promising for high-speed devices, with some potential for operation in the terahertz regime.[28,43,320] SWNT films consisting of aligned arrays represent the most realistic path to such devices.[321] This section summarizes recent efforts to measure and optimize the high-frequency response of SWNT TFTs, focusing on results obtained from conventional scattering-parameter measurements. Collections of devices configured as oscillators,[322] resonant antennas, RF amplifiers, mixers, and audio amplifiers provide examples of all of the key building blocks for RF analog electronics technology, with functional, all-nanotube transistor radios as demonstration systems.[323]

7.1. Measurement and Analysis of High-Frequency SWNT TFTs

Due to their relatively low impedance, direct scattering-parameter measurement of high-frequency properties of SWNT TFTs can be accomplished with standard high-frequency test equipment, thereby avoiding indirect measurement techniques that have been used in individual SWNT transistors.[207,324–327] In one approach, devices with L_Cs of 300 nm were formed with partially aligned SWNT deposited from solution by dielectrophoresis.[328] Although such devices show low on/off ratios (consistent with the enrichment of *m*-SWNT content via this deposition technique), their cutoff frequencies for current gain (f_t) are close to 4 GHz. The extracted "intrinsic" current gain and computed cut-off frequency for power gain (f_{max}) has some uncertainty, due to the very small intrinsic capacitance of SWNTs and less-than-unity stability factor for these films. Similar approaches can yield devices ($L_C \sim 800$ nm) on plastic (Fig. 18a inset), where f_t, is near ~1 GHz (Fig. 18a).[329]

Improved performance and reproducibility can be obtained in devices that use aligned SWNT arrays grown on quartz, with electrodes configured to match those of conventional ground-signal-ground (GSG) microwave probes (Fig. 18b and c).[323] The extracted cut-off frequency for a device with comparable but larger L_C, i.e., L_C of 700 nm, is 5 GHz for current gain and 9 GHz for power gain (Fig. 18d).[330] The achievement of ~10 GHz cut-off frequency for TFTs built on relatively low *D*, ca. ~5 SWNT μm^{-1}, SWNT aligned arrays, demonstrates the high quality of structurally perfect, pristine CVD nanotubes. The L_C scaling behavior of these transistors indicates that they are not dominated by contact resistance, for L_Cs in the micrometer range. The linear dependence of f_t on $1/L_C$ suggests a large effect of the capacitance associated with parasitics (Fig. 18e).[323] Effective ways to increase *D* and to dope nanotubes at the contacts are necessary to improve the performance, especially in the sub-100 nm regime.

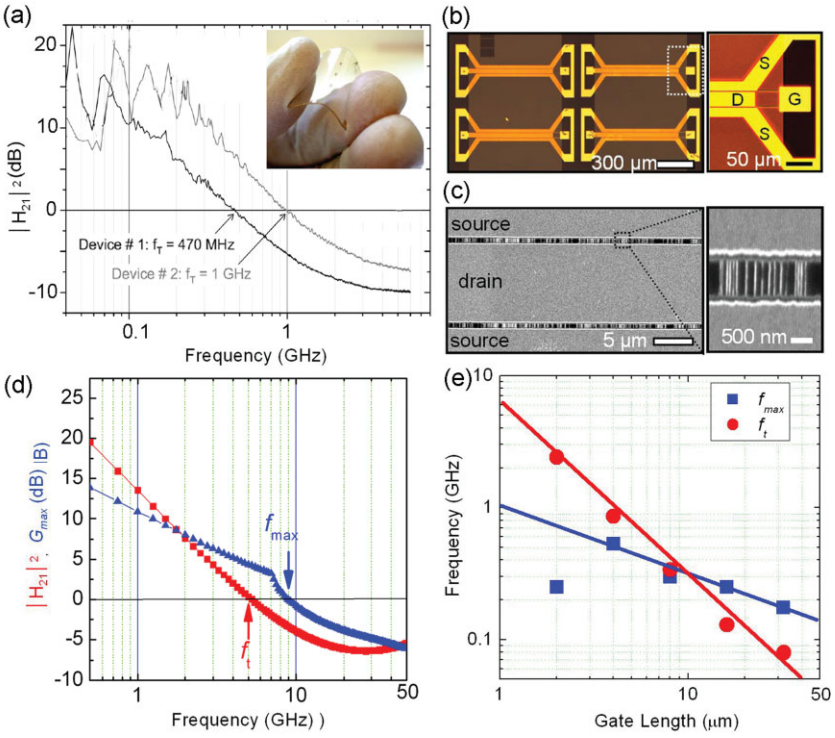

Figure 18. a) Current gain ($|H_{21}|^2$) as a function of frequency for two SWNT TFTs on a plastic substrate with L_C of 800 nm. Inset: optical image of high-frequency SWNT TFTs on plastic substrate. Reproduced with permission from Ref. [329]. Copyright 2007 American Institute of Physics. b) Optical image of SWNT TFT that uses aligned arrays of SWNTs grown on quartz and GSG layout designed for high-frequency measurements. Inset: magnified view showing the signal-ground-signal layout for probing pads. c) SEM image of SWNT arrays in the channel regions of device with split gate design. Inset: magnified view. d) $|H_{21}|^2$ and maximum power gain (G_{max}) as a function of frequency for a SWNT TFT with L_C of 700 nm. g) $|H_{21}|^2$ and G_{max} as a function of gate length for TFTs based on SWNT aligned arrays. Reproduced with permission from Ref. [323]. Copyright 2008 American Academy of Science.

7.2. Carbon-Nanotube Transistor Radio: A Functional High-Frequency System

Compared with digital electronics, analog systems require relatively low integration densities, especially for the highest performance parts. These aspects, the high mobilities and the potential for intrinsically linear behavior[331] in SWNT TFTs render analog RF electronics an attractive potential area of application. As described in the last section, SWNT TFTs can produce larger-than-unity power gain in the very-high-frequency (VHF) range. They can therefore be configured as RF power amplifiers and integrated together to form functional analog electronic systems, e.g., nanotube radios, where SWNT TFTs provide all of the active components (Fig. 19a).[323] To form a radio system, SWNT chips composed of several TFTs are connected to an external antenna and a speaker through wire bonding (Fig. 19b). Such radios are able to receive signals broadcast by commercial radio stations. The power spectrum of the output of the radio to a weather/traffic report appears in Fig. 19c.[323]

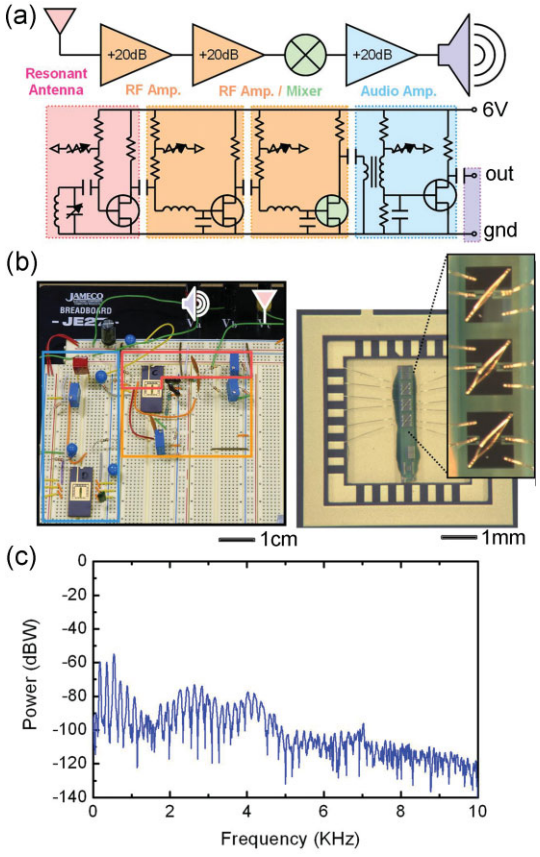

Figure 19. a) Block and circuit diagram of a radio system using SWNT TFTs for all of the active components. b) Optical image of the completed radio system, with magnified view of SWNT chips bonded into a package. c) Power spectrum of the radio output measured across an external speaker, for a commercial broadcast of a traffic report, showing a response characteristic of the human voice. Reproduced with permission from Ref. [323]. Copyright 2008 the National Academy of Sciences.

Similar to power amplifiers, oscillators, which represent another important component in analog RF systems, have been demonstrated with oscillation frequencies as high as 500 MHz.[322] We note that separate efforts recently demonstrated single-SWNT devices as mixers[332] and as mechanical oscillators[333] for certain components of different kinds of radios.

8. Conclusion and Outlook

Individual SWNTs provide an ideal 1D model system to study physics at the nanoscale. For practical electronic-device applications, thin films of SWNT, in the form of either random networks or aligned arrays, presently appear to represent the most realistic integration path. Compared with conventional materials, SWNT films have many interesting properties, rendering them suitable for various unusual multifunctional/multipurpose systems that require a combination of electrical, mechanical, optical, and chemical properties. Examples include transparent electronics, chemical sensors, and flexible electronics. In these cases, SWNTs could provide capabilities that are impossible or difficult to achieve with established inorganic materials, e.g., Si or III-Vs, as developed for wafer-based electronics.

In the past few years, research on SWNT thin films has evolved from fundamental studies and demonstrations of basic device operations to practical issues, such as performance advantages over existing technologies, cost, and manufacturability, evaluated in prototype systems that include ICs, transistor radios, and integrated sensor systems. In the simplest case, SWNT conductive coatings can now achieve levels of transparency and sheet conductance/mobility comparable with those of metal oxides, but with advantages in mechanical robustness, materials availability, and ease of forming coatings over large areas. Also, SWNT chemical sensors offer compelling detection capabilities compared to established technologies, with the interesting possibility for natural integration with other classes of SWNT film devices. For applications in active electronics, SWNT thin films can be assembled on a variety of substrates, including flexible sheets of plastic and stretchable slabs of rubber. Mobilities of transistors that use aligned arrays of SWNTs, where progress has been driven mainly by the development of guided-growth techniques, have reached levels (ca. >2000 cm^2 V^{-1} s^{-1}) that compare well with some of the best inorganic semiconductors. In parallel, research on devices that use random networks films have yielded mobilities (ca. $\sim$100 cm^2 V^{-1} s^{-1}) much larger than those of organic semiconductors/a-Si, as well as strategies for engineering the layouts of the networks for on/off ratios as high as 10^5, even in the presence of the usual population of *m*-SWNTs. In either type of film, polarity control can be readily achieved with charge-transfer doping methods, with demonstrations in power efficient CMOS logic gates. Gate dielectric materials have also been developed to decrease operating gate voltages to as low as $\sim$1 V and, in related work, to reduce the hysteresis from levels so large that the transistors could be used effectively as memory devices[334–336] to values that are nearly negligible. Both bottom-up, that is, heterogeneous percolative modeling, and top-down, that is, empirical device modeling, approaches have been developed to describe the behavior of SWNT devices/circuits quantitatively and predictively, for operating frequencies that range from direct current to tens of GHz. Complex functional digital and analog circuits, composed of up to nearly one hundred SWNT devices and operating at frequencies well into the GHz regime, respectively, have also been demonstrated, showing the scalability of SWNT thin-film technology. Procedures have also been developed for integrating SWNT TFTs into 3D formats and with other inorganic semiconductor devices, such as Si MOSFETs, thereby creating new application possibilities.[65]

In spite of this progress, significant challenges remain, especially with certain material aspects. First, and perhaps most important, techniques for growing electronically homogeneous SWNTs, or for post-growth purification, in a scalable and high-speed manner that can be applied with tubes in bulk or wafer-scale configurations must be developed. Second, advanced film-preparation methods are needed to achieve improved control over *D*, SWNT lengths, diameters, and orientation distributions, as these parameters heavily influence the properties of SWNT thin films. Third, techniques are required for controlled doping of SWNTs, for the purpose of increasing their conductivity, reducing parasitic contact resistances, and adjusting device V_Ts. Even if these problems are overcome, it is important to note that other

classes of materials, such as inorganic nanoparticle/nanowire/nanomembrane thin films[337–345] and graphene films,[346–350] might be able to provide alternatives to SWNTs, at least for certain applications. Nevertheless, in our view, recent progress suggests that SWNT films offer a unique combination of properties, such that the selected applications, cost structures, addressable markets, and related issues will ultimately determine the success of this material, rather than any intrinsic limitation associated with the physics or materials science.

Acknowledgements

We thank T. Banks, K. Colravy, and D. Sievers for help with the processing. This work was supported by DARPA-funded AFRL-managed Macroelectronics Program Contract FA8650- 04-C-7101, the National Science Foundation (NSF) through grant NIRT- 0403489, the U.S. Department of Energy through grant DE-FG02- 07ER46471, the Frederick Seitz Materials Research Lab and the Center for Microanalysis of Materials in University of Illinois, which is funded by U.S. Department of Energy through grant DE-FG02-07ER46453 and DE-FG02-07ER46471, the Center for Nanoscale Chemical Electrical Mechanical Manufacturing Systems in University of Illinois, which is funded by the NSF through grant DMI-0328162, Motorola Inc., Intel Corp., DuPont Corp., Northrop Grumman, and a fellowship support from the chemistry department (Q.C.).

Received: July 15, 2008
Revised: September 23, 2008

[1] P. Avouris, *Acc. Chem. Res.* **2002**, *35*, 1026.
[2] M. Ouyang, J. L. Huang, C. M. Lieber, *Acc. Chem. Res.* **2002**, *35*, 1018.
[3] V. N. Popov, *Mater. Sci. Eng, R* **2004**, *43*, 61.
[4] J. C. Charlier, X. Blase, S. Roche, *Rev. Mod. Phys.* **2007**, *79*, 677.
[5] T. Yamamoto, K. Watanabe, E. R. Hernandez, *Carbon Nanotubes* **2008**, *111*, 165.
[6] H. J. Dai, *Acc. Chem. Res.* **2002**, *35*, 1035.
[7] X. J. Zhou, J. Y. Park, S. M. Huang, J. Liu, P. L. McEuen, *Phys. Rev. Lett.* **2005**, *95*, 146805.
[8] C. T. White, T. N. Todorov, *Nature* **1998**, *393*, 240.
[9] B. M. Quinn, S. G. Lemay, *Adv. Mater.* **2006**, *18*, 855.
[10] A. Naeemi, J. D. Meindl, *IEEE Trans. Electron. Devices* **2007**, *54*, 26.
[11] H. Cho, K. H. Koo, P. Kapur, K. C. Saraswat, *IEEE Electron. Device Lett.* **2008**, *29*, 122.
[12] Z. Yao, C. L. Kane, C. Dekker, *Phys. Rev. Lett.* **2000**, *84*, 2941.
[13] E. Pop, D. Mann, Q. Wang, K. Goodson, H. J. Dai, *Nano Lett.* **2006**, *6*, 96.
[14] M. F. Yu, O. Lourie, M. J. Dyer, K. Moloni, T. F. Kelly, R. S. Ruoff, *Science* **2000**, *287*, 637.
[15] Z. W. Pan, S. S. Xie, L. Lu, B. H. Chang, L. F. Sun, W. Y. Zhou, G. Wang, D. L. Zhang, *Appl. Phys. Lett.* **1999**, *74*, 3152.
[16] P. Poncharal, Z. L. Wang, D. Ugarte, W. A. de Heer, *Science* **1999**, *283*, 1513.
[17] J. P. Salvetat, G. A. D. Briggs, J. M. Bonard, R. R. Bacsa, A. J. Kulik, T. Stockli, N. A. Burnham, L. Forro, *Phys. Rev. Lett.* **1999**, *82*, 944.
[18] E. W. Wong, P. E. Sheehan, C. M. Lieber, *Science* **1997**, *277*, 1971.
[19] M. M. J. Treacy, T. W. Ebbesen, J. M. Gibson, *Nature* **1996**, *381*, 678.
[20] D. Y. Khang, J. L. Xiao, C. Kocabas, S. MacLaren, T. Banks, H. Q. Jiang, Y. Y. G. Huang, J. A. Rogers, *Nano Lett.* **2008**, *8*, 124.
[21] M. F. Yu, B. S. Files, S. Arepalli, R. S. Ruoff, *Phys. Rev. Lett.* **2000**, *84*, 5552.
[22] D. A. Walters, L. M. Ericson, M. J. Casavant, J. Liu, D. T. Colbert, K. A. Smith, R. E. Smalley, *Appl. Phys. Lett.* **1999**, *74*, 3803.
[23] S. Niyogi, M. A. Hamon, H. Hu, B. Zhao, P. Bhowmik, R. Sen, M. E. Itkis, R. C. Haddon, *Acc. Chem. Res.* **2002**, *35*, 1105.
[24] D. Tasis, N. Tagmatarchis, A. Bianco, M. Prato, *Chem. Rev.* **2006**, *106*, 1105.
[25] M. Cinke, J. Li, B. Chen, A. Cassell, L. Delzeit, J. Han, M. Meyyappan, *Chem. Phys. Lett.* **2002**, *365*, 69.
[26] H. S. P. Wong, *IBM J. Res. Dev.* **2002**, *46*, 133.
[27] S. E. Thompson, S. Parthasarathy, *Mater. Today* **2006**, *9*, 20.
[28] P. Avouris, Z. H. Chen, V. Perebeinos, *Nat. Nanotechnol.* **2007**, *2*, 605.
[29] W. B. Choi, D. S. Chung, J. H. Kang, H. Y. Kim, Y. W. Jin, I. T. Han, Y. H. Lee, J. E. Jung, N. S. Lee, G. S. Park, J. M. Kim, *Appl. Phys. Lett.* **1999**, *75*, 3129.
[30] H. M. Cheng, Q. H. Yang, C. Liu, *Carbon* **2001**, *39*, 1447.
[31] L. Schlapbach, A. Zuttel, *Nature* **2001**, *414*, 353.
[32] A. S. Arico, P. Bruce, B. Scrosati, J. M. Tarascon, W. van Schalkwijk, *Nat. Mater.* **2005**, *4*, 366.
[33] Z. Liu, M. Winters, M. Holodniy, H. J. Dai, *Angew. Chem. Int. Ed.* **2007**, *46*, 2023.
[34] M. Prato, K. Kostarelos, A. Bianco, *Acc. Chem. Res.* **2008**, *41*, 60.
[35] M. Freitag, J. C. Tsang, J. Kirtley, A. Carlsen, J. Chen, A. Troeman, H. Hilgenkamp, P. Avouris, *Nano Lett.* **2006**, *6*, 1425.
[36] J. Chen, V. Perebeinos, M. Freitag, J. Tsang, Q. Fu, J. Liu, P. Avouris, *Science* **2005**, *310*, 1171.
[37] K. Kordas, G. Toth, P. Moilanen, M. Kumpumaki, J. Vahakangas, A. Uusimaki, R. Vajtai, P. M. Ajayan, *Appl. Phys. Lett.* **2007**, *90*, 123105.
[38] T. Iwai, Y. Awano, *Fujitsu Sci. Tech. J.* **2007**, *43*, 508.
[39] G. F. Close, S. Yasuda, B. Paul, S. Fujita, H. S. P. Wong, *Nano Lett.* **2008**, *8*, 706.
[40] S. N. Kim, J. F. Rusling, F. Papadimitrakopoulos, *Adv. Mater.* **2007**, *19*, 3214.
[41] P. Avouris, J. Chen, *Mater. Today* **2006**, *9*, 46.
[42] A. P. Graham, G. S. Duesberg, W. Hoenlein, F. Kreupl, M. Liebau, R. Martin, B. Rajasekharan, W. Pamler, R. Seidel, W. Steinhoegl, E. Unger, *Appl. Phys. A-Mater. Sci. Process.* **2005**, *80*, 1141.
[43] J. Appenzeller, *Proc. IEEE* **2008**, *96*, 201.
[44] S. A. Wolf, D. D. Awschalom, R. A. Buhrman, J. M. Daughton, S. von Molnar, M. L. Roukes, A. Y. Chtchelkanova, D. M. Treger, *Science* **2001**, *294*, 1488.
[45] I. Zutic, J. Fabian, S. Das Sarma, *Rev. Mod. Phys.* **2004**, *76*, 323.
[46] D. D. Awschalom, M. E. Flatte, *Nat. Phys.* **2007**, *3*, 153.
[47] C. Felser, G. H. Fecher, B. Balke, *Angew. Chem. Int. Ed.* **2007**, *46*, 668.
[48] C. Joachim, J. K. Gimzewski, A. Aviram, *Nature* **2000**, *408*, 541.
[49] J. M. Tour, *Acc. Chem. Res.* **2000**, *33*, 791.
[50] F. M. Raymo, *Adv. Mater.* **2002**, *14*, 401.
[51] D. Vulillaume, *C. R. Phys.* **2008**, *9*, 78.
[52] J. E. Green, J. W. Choi, A. Boukai, Y. Bunimovich, E. Johnston-Halperin, E. DeIonno, Y. Luo, B. A. Sheriff, K. Xu, Y. S. Shin, H. R. Tseng, J. F. Stoddart, J. R. Heath, *Nature* **2007**, *445*, 414.
[53] A. H. Flood, J. F. Stoddart, D. W. Steuerman, J. R. Heath, *Science* **2004**, *306*, 2055.
[54] J. Huang, M. Momenzadeh, F. Lombardi, *IEEE Des. Test Comput.* **2007**, *24*, 304.
[55] P. J. Kuekes, D. R. Stewart, R. S. Williams, *J. Appl. Phys.* **2005**, *97*, 034301.
[56] Y. Chen, G. Y. Jung, D. A. A. Ohlberg, X. M. Li, D. R. Stewart, J. O. Jeppesen, K. A. Nielsen, J. F. Stoddart, R. S. Williams, *Nanotechnology* **2003**, *14*, 462.
[57] N. A. Melosh, A. Boukai, F. Diana, B. Gerardot, A. Badolato, P. M. Petroff, J. R. Heath, *Science* **2003**, *300*, 112.
[58] Y. Cui, C. M. Lieber, *Science* **2001**, *291*, 851.
[59] T. Rueckes, K. Kim, E. Joselevich, G. Y. Tseng, C. L. Cheung, C. M. Lieber, *Science* **2000**, *289*, 94.
[60] W. Lu, C. M. Lieber, *Nat. Mater.* **2007**, *6*, 841.

[61] A. Javey, H. Kim, M. Brink, Q. Wang, A. Ural, J. Guo, P. McIntyre, P. McEuen, M. Lundstrom, H. J. Dai, *Nat. Mater.* **2002**, *1*, 241.
[62] P. J. Burke, *Solid-State Electron.* **2004**, *48*, 1981.
[63] Z. H. Chen, J. Appenzeller, Y. M. Lin, J. Sippel-Oakley, A. G. Rinzler, J. Y. Tang, S. J. Wind, P. M. Solomon, P. Avouris, *Science* **2006**, *311*, 1735.
[64] S. J. Kang, C. Kocabas, T. Ozel, M. Shim, N. Pimparkar, M. A. Alam, S. V. Rotkin, J. A. Rogers, *Nat. Nanotechnol.* **2007**, *2*, 230.
[65] J. H. Ahn, H. S. Kim, K. J. Lee, S. Jeon, S. J. Kang, Y. G. Sun, R. G. Nuzzo, J. A. Rogers, *Science* **2006**, *314*, 1754.
[66] Q. Cao, H. S. Kim, N. Pimparkar, J. P. Kulkarni, C. J. Wang, M. Shim, K. Roy, M. A. Alam, J. A. Rogers, *Nature* **2008**, *454*, 495.
[67] R. H. Reuss, B. R. Chalamala, A. Moussessian, M. G. Kane, A. Kumar, D. C. Zhang, J. A. Rogers, M. Hatalis, D. Temple, G. Moddel, B. J. Eliasson, M. J. Estes, J. Kunze, E. S. Handy, E. S. Harmon, D. B. Salzman, J. M. Woodall, M. A. Alam, J. Y. Murthy, S. C. Jacobsen, M. Olivier, D. Markus, P. M. Campbell, E. Snow, *Proc. IEEE* **2005**, *93*, 1239.
[68] T. V. Sreekumar, T. Liu, S. Kumar, L. M. Ericson, R. H. Hauge, R. E. Smalley, *Chem. Mater.* **2003**, *15*, 175.
[69] L. Hu, D. S. Hecht, G. Grüner, *Nano Lett.* **2004**, *4*, 2513.
[70] M. Burghard, G. Duesberg, G. Philipp, J. Muster, S. Roth, *Adv. Mater.* **1998**, *10*, 584.
[71] M. D. Lay, J. P. Novak, E. S. Snow, *Nano Lett.* **2004**, *4*, 603.
[72] S. G. Rao, L. Huang, W. Setyawan, S. H. Hong, *Nature* **2003**, *425*, 36.
[73] H. Shimoda, S. J. Oh, H. Z. Geng, R. J. Walker, X. B. Zhang, L. E. McNeil, O. Zhou, *Adv. Mater.* **2002**, *14*, 899.
[74] G. S. Tulevski, J. Hannon, A. Afzali, Z. Chen, P. Avouris, C. R. Kagan, *J. Am. Chem. Soc.* **2007**, *129*, 1164.
[75] M. Lee, J. Im, B. Y. Lee, S. Myung, J. Kang, L. Huang, Y. K. Kwon, S. Hong, *Nat. Nanotechnol.* **2006**, *1*, 66.
[76] Z. Wu, Z. Chen, X. Du, J. M. Logan, J. Sippel, M. Nikolou, K. Kamaras, J. R. Reynolds, D. B. Tanner, A. F. Hebard, A. G. Rinzler, *Science* **2004**, *305*, 1273.
[77] Y. X. Zhou, L. B. Hu, G. Grüner, *Appl. Phys. Lett.* **2006**, *88*, 123109.
[78] M. A. Meitl, Y. X. Zhou, A. Gaur, S. Jeon, M. L. Usrey, M. S. Strano, J. A. Rogers, *Nano Lett.* **2004**, *4*, 1643.
[79] J. U. Park, M. A. Meitl, S. H. Hur, M. L. Usrey, M. S. Strano, P. J. A. Kenis, J. A. Rogers, *Angew. Chem. Int. Ed.* **2006**, *45*, 581.
[80] M. S. Fuhrer, J. Nygard, L. Shih, M. Forero, Y. G. Yoon, M. S. C. Mazzoni, H. J. Choi, J. Ihm, S. G. Louie, A. Zettl, P. L. McEuen, *Science* **2000**, *288*, 494.
[81] A. A. Odintsov, *Phys. Rev. Lett.* **2000**, *85*, 150.
[82] S. Banerjee, B. E. White, L. M. Huang, B. J. Rego, S. O'Brien, I. P. Herman, *J. Vac. Sci. Technol. B* **2006**, *24*, 3173.
[83] X. Q. Chen, T. Saito, H. Yamada, K. Matsushige, *Appl. Phys. Lett.* **2001**, *78*, 3714.
[84] M. R. Diehl, S. N. Yaliraki, R. A. Beckman, M. Barahona, J. R. Heath, *Angew. Chem. Int. Ed.* **2001**, *41*, 353.
[85] L. A. Nagahara, I. Amlani, J. Lewenstein, R. K. Tsui, *Appl. Phys. Lett.* **2002**, *80*, 3826.
[86] R. Krupke, F. Hennrich, H. von Lohneysen, M. M. Kappes, *Science* **2003**, *301*, 344.
[87] R. Krupke, S. Linden, M. Rapp, F. Hennrich, *Adv. Mater.* **2006**, *18*, 1468.
[88] J. E. Fischer, W. Zhou, J. Vavro, M. C. Llaguno, C. Guthy, R. Haggenmueller, M. J. Casavant, D. E. Walters, R. E. Smalley, *J. Appl. Phys.* **2003**, *93*, 2157.
[89] D. P. Long, J. L. Lazorcik, R. Shashidhar, *Adv. Mater.* **2004**, *16*, 814.
[90] X. Xiong, L. Jaberansari, M. G. Hahm, A. Busnaina, Y. J. Jung, *Small* **2007**, *3*, 2006.
[91] G. H. Yu, A. Y. Cao, C. M. Lieber, *Nat. Nanotechnol.* **2007**, *2*, 372.
[92] G. H. Yu, X. L. Li, C. M. Lieber, A. Y. Cao, *J. Mater. Chem.* **2008**, *18*, 728.
[93] M. D. Lima, M. J. de Andrade, C. P. Bergmann, S. Roth, *J. Mater. Chem.* **2008**, *18*, 776.
[94] H. Ko, V. V. Tsukruk, *Nano Lett.* **2006**, *6*, 1443.
[95] X. L. Li, L. Zhang, X. R. Wang, I. Shimoyama, X. M. Sun, W. S. Seo, H. J. Dai, *J. Am. Chem. Soc.* **2007**, *129*, 4890.
[96] S. J. Kang, C. Kocabas, H. S. Kim, Q. Cao, M. A. Meitl, D. Y. Khang, J. A. Rogers, *Nano Lett.* **2007**, *7*, 3343.
[97] P. Beecher, P. Servati, A. Rozhin, A. Colli, V. Scardaci, S. Pisana, T. Hasan, A. J. Flewitt, J. Robertson, G. W. Hsieh, F. M. Li, A. Nathan, A. C. Ferrari, W. I. Milne, *J. Appl. Phys.* **2007**, *102*, 043710.
[98] J. U. Park, M. Hardy, S. J. Kang, K. Barton, K. Adair, D. K. Mukhopadhyay, C. Y. Lee, M. S. Strano, A. G. Alleyne, J. G. Georgiadis, P. M. Ferreira, J. A. Rogers, *Nat. Mater.* **2007**, *6*, 782.
[99] K. Kordas, T. Mustonen, G. Toth, H. Jantunen, M. Lajunen, C. Soldano, S. Talapatra, S. Kar, R. Vajtai, P. M. Ajayan, *Small* **2006**, *2*, 1021.
[100] Y. L. Li, L. H. Zhang, X. H. Zhong, A. H. Windle, *Nanotechnology* **2007**, *18*, 225604.
[101] S. Maruyama, R. Kojima, Y. Miyauchi, S. Chiashi, M. Kohno, *Chem. Phys. Lett.* **2002**, *360*, 229.
[102] J. P. Edgeworth, N. R. Wilson, J. V. Macpherson, *Small* **2007**, *3*, 860.
[103] K. Hata, D. N. Futaba, K. Mizuno, T. Namai, M. Yumura, S. Iijima, *Science* **2004**, *306*, 1362.
[104] G. Y. Zhang, D. Mann, L. Zhang, A. Javey, Y. M. Li, E. Yenilmez, Q. Wang, J. P. McVittie, Y. Nishi, J. Gibbons, H. J. Dai, *Proc. Natl. Acad. Sci. U. S. A.* **2005**, *102*, 16141.
[105] Y. Murakami, S. Chiashi, Y. Miyauchi, M. H. Hu, M. Ogura, T. Okubo, S. Maruyama, *Chem. Phys. Lett.* **2004**, *385*, 298.
[106] Q. Cao, S.-H. Hur, Z.-T. Zhu, Y. Sun, C. Wang, M. A. Meitl, M. Shim, J. A. Rogers, *Adv. Mater.* **2006**, *18*, 304.
[107] C. L. Cheung, A. Kurtz, H. Park, C. M. Lieber, *J. Phys. Chem. B* **2002**, *106*, 2429.
[108] G. S. Duesberg, A. P. Graham, M. Liebau, R. Seidel, E. Unger, F. Kreupl, W. Hoenlein, *Nano Lett.* **2003**, *3*, 257.
[109] M. Ishida, H. Hongo, F. Nihey, Y. Ochiai, *Jpn. J. Appl. Phys. Part 2* **2004**, *43*, L1356.
[110] Y. M. Li, W. Kim, Y. G. Zhang, M. Rolandi, D. W. Wang, H. J. Dai, *J. Phys. Chem. B* **2001**, *105*, 11424.
[111] X. Liu, T. P. Bigioni, Y. Xu, A. M. Cassell, B. A. Cruden, *J. Phys. Chem. B* **2006**, *110*, 20102.
[112] K. M. Ryu, A. Badmaev, L. Gomez, F. Ishikawa, B. Lei, C. W. Zhou, *J. Am. Chem. Soc.* **2007**, *129*, 10104.
[113] S. M. Bachilo, L. Balzano, J. E. Herrera, F. Pompeo, D. E. Resasco, R. B. Weisman, *J. Am. Chem. Soc.* **2003**, *125*, 11186.
[114] D. Ciuparu, Y. Chen, S. Lim, G. L. Haller, L. Pfefferle, *J. Phys. Chem. B* **2004**, *108*, 503.
[115] B. Wang, C. H. P. Poa, L. Wei, L. J. Li, Y. H. Yang, Y. Chen, *J. Am. Chem. Soc.* **2007**, *129*, 9014.
[116] B. Wang, L. Wei, L. Yao, L. J. Li, Y. H. Yang, Y. Chen, *J. Phys. Chem. C* **2007**, *111*, 14612.
[117] B. B. Wang, S. Lee, X. Z. Xu, S. H. Choi, H. Yan, B. Zhang, W. Hao, *Appl. Surf. Sci.* **2004**, *236*, 6.
[118] Y. T. Lee, N. S. Kim, J. Park, J. B. Han, Y. S. Choi, H. Ryu, H. J. Lee, *Chem. Phys. Lett.* **2003**, *372*, 853.
[119] E. Joselevich, C. M. Lieber, *Nano Lett.* **2002**, *2*, 1137.
[120] Y. G. Zhang, A. L. Chang, J. Cao, Q. Wang, W. Kim, Y. M. Li, N. Morris, E. Yenilmez, J. Kong, H. J. Dai, *Appl. Phys. Lett.* **2001**, *79*, 3155.
[121] S. M. Huang, M. Woodson, R. Smalley, J. Liu, *Nano Lett.* **2004**, *4*, 1025.
[122] S. M. Huang, X. Y. Cai, J. Liu, *J. Am. Chem. Soc.* **2003**, *125*, 5636.
[123] Z. Jin, H. B. Chu, J. Y. Wang, J. X. Hong, W. C. Tan, Y. Li, *Nano Lett.* **2007**, *7*, 2073.
[124] L. M. Huang, B. White, M. Y. Sfeir, M. Y. Huang, H. X. Huang, S. Wind, J. Hone, S. O'Brien, *J. Phys. Chem. B* **2006**, *110*, 11103.
[125] S. M. Huang, B. Maynor, X. Y. Cai, J. Liu, *Adv. Mater.* **2003**, *15*, 1651.
[126] A. Ismach, L. Segev, E. Wachtel, E. Joselevich, *Angew. Chem. Int. Ed.* **2004**, *43*, 6140.
[127] A. Ismach, D. Kantorovich, E. Joselevich, *J. Am. Chem. Soc.* **2005**, *127*, 11554.
[128] C. Kocabas, S. H. Hur, A. Gaur, M. A. Meitl, M. Shim, J. A. Rogers, *Small* **2005**, *1*, 1110.

[129] S. Han, X. L. Liu, C. W. Zhou, *J. Am. Chem. Soc.* **2005**, *127*, 5294.
[130] C. Kocabas, S. J. Kang, T. Ozel, M. Shim, J. A. Rogers, *J. Phys. Chem. C* **2007**, *111*, 17879.
[131] L. Ding, D. N. Yuan, J. Liu, *J. Am. Chem. Soc.* **2008**, *130*, 5428.
[132] C. Kocabas, M. Shim, J. A. Rogers, *J. Am. Chem. Soc.* **2006**, *128*, 4540.
[133] A. Ismach, E. Joselevich, *Nano Lett.* **2006**, *6*, 1706.
[134] H. Ago, K. Imamoto, N. Ishigami, R. Ohdo, K. Ikeda, M. Tsuji, *Appl. Phys. Lett.* **2007**, *90*, 123112.
[135] N. Geblinger, A. Ismach, E. Joselevich, *Nat. Nanotechnol.* **2008**, *3*, 195.
[136] Y. M. Li, D. Mann, M. Rolandi, W. Kim, A. Ural, S. Hung, A. Javey, J. Cao, D. W. Wang, E. Yenilmez, Q. Wang, J. F. Gibbons, Y. Nishi, H. J. Dai, *Nano Lett.* **2004**, *4*, 317.
[137] Y. M. Li, S. Peng, D. Mann, J. Cao, R. Tu, K. J. Cho, H. J. Dai, *J. Phys. Chem. B* **2005**, *109*, 6968.
[138] M. C. Hersam, *Nat. Nanotechnol.* **2008**, *3*, 387.
[139] P. G. Collins, M. Hersam, M. Arnold, R. Martel, P. Avouris, *Phys. Rev. Lett.* **2001**, *86*, 3128.
[140] P. C. Collins, M. S. Arnold, P. Avouris, *Science* **2001**, *292*, 706.
[141] R. V. Seidel, A. P. Graham, B. Rajasekharan, E. Unger, M. Liebau, G. S. Duesberg, F. Kreupl, W. Hoenlein, *J. Appl. Phys.* **2004**, *96*, 6694.
[142] Y. X. Zhou, A. Gaur, S. H. Hur, C. Kocabas, M. A. Meitl, M. Shim, J. A. Rogers, *Nano Lett.* **2004**, *4*, 2031.
[143] M. Zheng, A. Jagota, E. D. Semke, B. A. Diner, R. S. McLean, S. R. Lustig, R. E. Richardson, N. G. Tassi, *Nat. Mater.* **2003**, *2*, 338.
[144] V. C. Moore, M. S. Strano, E. H. Haroz, R. H. Hauge, R. E. Smalley, J. Schmidt, Y. Talmon, *Nano Lett.* **2003**, *3*, 1379.
[145] M. Zheng, A. Jagota, M. S. Strano, A. P. Santos, P. Barone, S. G. Chou, B. A. Diner, M. S. Dresselhaus, R. S. Mclean, G. B. Onoa, G. G. Samsonidze, E. D. Semke, M. Usrey, D. J. Walls, *Science* **2003**, *302*, 1545.
[146] M. S. Strano, M. Zheng, A. Jagota, G. B. Onoa, D. A. Heller, P. W. Barone, M. L. Usrey, *Nano. Lett.* **2004**, *4*, 543.
[147] M. S. Arnold, A. A. Green, J. F. Hulvat, S. I. Stupp, M. C. Hersam, *Nat. Nanotechnol.* **2006**, *1*, 60.
[148] S. Y. Ju, J. Doll, I. Sharma, F. Papadimitrakopoulos, *Nat. Nanotechnol.* **2008**, *3*, 356.
[149] M. Zheng, E. D. Semke, *J. Am. Chem. Soc.* **2007**, *129*, 6084.
[150] L. Zhang, S. Zaric, X. M. Tu, X. R. Wang, W. Zhao, H. J. Dai, *J. Am. Chem. Soc.* **2008**, *130*, 2686.
[151] X. L. Li, X. M. Tu, S. Zaric, K. Welsher, W. S. Seo, W. Zhao, H. J. Dai, *J. Am. Chem. Soc.* **2007**, *129*, 15770.
[152] J. A. Fagan, M. L. Becker, J. Chun, E. K. Hobbie, *Adv. Mater.* **2008**, *20*, 1609.
[153] N. Lzard, S. Kazaoui, K. Hata, T. Okazaki, T. Saito, S. Iijima, N. Minami, *Appl. Phys. Lett.* **2008**, *92*, 243112.
[154] D. Chattopadhyay, I. Galeska, F. Papadimitrakopoulos, *J. Am. Chem. Soc.* **2003**, *125*, 3370.
[155] A. Nish, J. Y. Hwang, J. Doig, R. J. Nicholas, *Nat. Nanotechnol.* **2007**, *2*, 640.
[156] M. C. LeMieux, M. Roberts, S. Barman, Y. W. Jin, J. M. Kim, Z. N. Bao, *Science* **2008**, *321*, 101.
[157] H. Li, B. Zhou, Y. Lin, L. Gu, W. Wang, K. A. S. Fernando, S. Kumar, L. F. Allard, Y.-P. Sun, *J. Am. Chem. Soc.* **2004**, *126*, 1014.
[158] K. H. An, J. S. Park, C. M. Yang, S. Y. Jeong, S. C. Lim, C. Kang, J. H. Son, M. S. Jeong, Y. H. Lee, *J. Am. Chem. Soc.* **2005**, *127*, 5196.
[159] C. M. Yang, J. S. Park, K. H. An, S. C. Lim, K. Seo, B. Kim, K. A. Park, S. Han, C. Y. Park, Y. H. Lee, *J. Phys. Chem. B* **2005**, *109*, 19242.
[160] Y. Miyata, Y. Maniwa, H. Kataura, *J. Phys. Chem. B* **2006**, *110*, 25.
[161] C. M. Yang, K. H. An, J. S. Park, K. A. Park, S. C. Lim, S. H. Cho, Y. S. Lee, W. Park, C. Y. Park, Y. H. Lee, *Phys. Rev. B* **2006**, *73*, 075418.
[162] H. M. So, B. K. Kim, D. W. Park, B. S. Kim, J. J. Kim, K. J. Kong, H. J. Chang, J. O. Lee, *J. Am. Chem. Soc.* **2007**, *129*, 4866.
[163] D. Wunderlich, F. Hauke, A. Hirsch, *J. Mater. Chem.* **2008**, *18*, 1493.
[164] D. Wunderlich, F. Hauke, A. Hirsch, *Chem. Eur. J.* **2008**, *14*, 1607.
[165] M. S. Strano, C. A. Dyke, M. L. Usrey, P. W. Barone, M. J. Allen, H. Shan, C. Kittrell, R. H. Hauge, J. M. Tour, R. E. Smalley, *Science* **2003**, *301*, 1519.
[166] H. Park, J. J. Zhao, J. P. Lu, *Nanotechnology* **2005**, *16*, 635.
[167] C. J. Wang, Q. Cao, T. Ozel, A. Gaur, J. A. Rogers, M. Shim, *J. Am. Chem. Soc.* **2005**, *127*, 11460.
[168] G. Y. Zhang, P. F. Qi, X. R. Wang, Y. R. Lu, X. L. Li, R. Tu, S. Bangsaruntip, D. Mann, L. Zhang, H. J. Dai, *Science* **2006**, *314*, 974.
[169] C. Kocabas, M. A. Meitl, A. Gaur, M. Shim, J. A. Rogers, *Nano Lett.* **2004**, *4*, 2421.
[170] K. Maehashi, Y. Ohno, K. Inoue, K. Matsumoto, *Appl. Phys. Lett.* **2004**, *85*, 858.
[171] H. J. Huang, R. Maruyama, K. Noda, H. Kajiura, K. Kadono, *J. Phys. Chem. B* **2006**, *110*, 7316.
[172] H. Xu, S. X. Zhang, S. M. Anlage, L. B. Hu, G. Gruner, *Phys. Rev. B* **2008**, *77*.
[173] G. Gruner, *J. Mater. Chem.* **2006**, *16*, 3533.
[174] N. Saran, K. Parikh, D. S. Suh, E. Munoz, H. Kolla, S. K. Manohar, *J. Am. Chem. Soc.* **2004**, *126*, 4462.
[175] M. Kaempgen, G. S. Duesberg, S. Roth, *Appl. Surf. Sci.* **2005**, *252*, 425.
[176] D. Hecht, L. B. Hu, G. Gruner, *Appl. Phys. Lett.* **2006**, *89*, 133112.
[177] B. Vigolo, C. Coulon, M. Maugey, C. Zakri, P. Poulin, *Science* **2005**, *309*, 920.
[178] M. A. Alam, N. Pimparkar, S. Kumar, J. Murthy, *MRS Bull.* **2006**, *31*, 466.
[179] S. Kumar, M. A. Alam, J. Y. Murthy, *J. Heat Transf. Trans. ASME* **2007**, *129*, 500.
[180] S. Kumar, J. Y. Murthy, M. A. Alam, *Phys. Rev. Lett.* **2005**, *95*, 066802.
[181] S. Kumar, N. Pimparkar, J. Y. Murthy, M. A. Alam, *Appl. Phys. Lett.* **2006**, *88*, 123505.
[182] N. Pimparkar, Q. Cao, J. A. Rogers, M. A. Alam, **2008**, Unpublished results.
[183] C. Kocabas, N. Pimparkar, O. Yesilyurt, S. J. Kang, M. A. Alam, J. A. Rogers, *Nano Lett.* **2007**, *7*, 1195.
[184] N. Pimparkar, C. Kocabas, S. J. Kang, J. Rogers, M. A. Alam, *IEEE Electron Device Lett.* **2007**, *28*, 593.
[185] N. Pimparkar, Q. Cao, S. Kumar, J. Y. Murthy, J. Rogers, M. A. Alam, *IEEE Electron Device Lett.* **2007**, *28*, 157.
[186] N. Pimparkar, J. Guo, M. A. Alam, *IEEE Trans. Electron. Devices* **2007**, *54*, 637.
[187] J. Guo, S. Goasguen, M. Lundstrom, S. Datta, *Appl. Phys. Lett.* **2002**, *81*, 1486.
[188] O. Wunnicke, *Appl. Phys. Lett.* **2006**, *89*, 083102.
[189] Q. Cao, M. G. Xia, C. Kocabas, M. Shim, J. A. Rogers, S. V. Rotkin, *Appl. Phys. Lett.* **2007**, *90*, 023516.
[190] S. Heinze, J. Tersoff, R. Martel, V. Derycke, J. Appenzeller, P. Avouris, *Phys. Rev. Lett.* **2002**, *89*, 106801.
[191] J. Appenzeller, Y. M. Lin, J. Knoch, Z. H. Chen, P. Avouris, *IEEE Trans. Electron. Devices* **2005**, *52*, 2568.
[192] Z. H. Chen, J. Appenzeller, J. Knoch, Y. M. Lin, P. Avouris, *Nano Lett.* **2005**, *5*, 1497.
[193] A. Javey, J. Guo, Q. Wang, M. Lundstrom, H. Dai, *Nature* **2003**, *424*, 654.
[194] S. D. Li, Z. Yu, C. Rutherglen, P. J. Burke, *Nano Lett.* **2004**, *4*, 2003.
[195] T. Durkop, S. A. Getty, E. Cobas, M. S. Fuhrer, *Nano Lett.* **2004**, *4*, 35.
[196] T. Ozel, A. Gaur, J. A. Rogers, M. Shim, *Nano Lett.* **2005**, *5*, 905.
[197] S.-H. Hur, C. Kocabas, A. Gaur, M. Shim, O. O. Park, J. A. Rogers, *J. Apply. Phys.* **2005**, *98*, 114302.
[198] Q. Cao, M. G. Xia, M. Shim, J. A. Rogers, *Adv. Funct. Mater.* **2006**, *16*, 2355.
[199] S. Luan, G. W. Neudeck, *J. Appl. Phys.* **1992**, *72*, 766.
[200] J. Chen, C. Klinke, A. Afzali, P. Avouris, *Appl. Phys. Lett.* **2005**, *86*, 123108.
[201] C. Klinke, A. Afzali, P. Avouris, *Chem. Phys. Lett.* **2006**, *430*, 75.
[202] A. Javey, J. Guo, D. B. Farmer, Q. Wang, D. W. Wang, R. G. Gordon, M. Lundstrom, H. J. Dai, *Nano Lett.* **2004**, *4*, 447.
[203] Y. Nosho, Y. Ohno, S. Kishimoto, T. Mizutani, *Appl. Phys. Lett.* **2005**, *86*, 073105.

[204] J. Kong, N. R. Franklin, C. W. Zhou, M. G. Chapline, S. Peng, K. J. Cho, H. J. Dai, *Science* **2000**, *287*, 622.
[205] P. G. Collins, K. Bradley, M. Ishigami, A. Zettl, *Science* **2000**, *287*, 1801.
[206] D. Kaminishi, H. Ozaki, Y. Ohno, K. Maehashi, K. Inoue, K. Matsumoto, Y. Seri, A. Masuda, H. Matsumura, *Appl. Phys. Lett.* **2005**, *86*, 113115.
[207] A. A. Pesetski, J. E. Baumgardner, E. Folk, J. X. Przybysz, J. D. Adam, H. Zhang, *Appl. Phys. Lett.* **2006**, *88*, 113103.
[208] J. J. Zhao, A. Buldum, J. Han, J. P. Lu, *Nanotechnology* **2002**, *13*, 195.
[209] D. C. Sorescu, K. D. Jordan, P. Avouris, *J. Phys. Chem. B* **2001**, *105*, 11227.
[210] S. H. Jhi, S. G. Louie, M. L. Cohen, *Phys. Rev. Lett.* **2000**, *85*, 1710.
[211] G. U. Sumanasekera, C. K. W. Adu, S. Fang, P. C. Eklund, *Phys. Rev. Lett.* **2000**, *85*, 1096.
[212] V. Derycke, R. Martel, J. Appenzeller, P. Avouris, *Appl. Phys. Lett.* **2002**, *80*, 2773.
[213] M. Shim, A. Javey, N. W. S. Kam, H. J. Dai, *J. Am. Chem. Soc.* **2001**, *123*, 11512.
[214] C. Klinke, J. Chen, A. Afzali, P. Avouris, *Nano Lett.* **2005**, *5*, 555.
[215] S. H. Hur, M. H. Yoon, A. Gaur, M. Shim, A. Facchetti, T. J. Marks, J. A. Rogers, *J. Am. Chem. Soc.* **2005**, *127*, 13808.
[216] M. Shim, T. Ozel, A. Gaur, C. J. Wang, *J. Am. Chem. Soc.* **2006**, *128*, 7522.
[217] T. B. Singh, N. S. Sariciftci, *Ann. Rev. Mater. Res.* **2006**, *36*, 199.
[218] C. R. Newman, C. D. Frisbie, D. A. da Silva, J. L. Bredas, P. C. Ewbank, K. R. Mann, *Chem. Mat.* **2004**, *16*, 4436.
[219] A. Facchetti, *Mater. Today* **2007**, *10*, 28.
[220] M. F. Islam, D. E. Milkie, C. L. Kane, A. G. Yodh, J. M. Kikkawa, *Phys. Rev. Lett.* **2004**, *93*, 037404.
[221] B. Yakobson, P. Avouris, *Topics Appl. Phys.* **2001**, *80*, 287.
[222] M. R. Falvo, G. J. Clary, R. M. Taylor, V. Chi, F. P. Brooks, S. Washburn, R. Superfine, *Nature* **1997**, *389*, 582.
[223] S.-H. Hur, O. O. Park, J. A. Rogers, *Appl. Phys. Lett.* **2005**, *86*, 243502.
[224] J. F. Wager, *Science* **2003**, *300*, 1245.
[225] Y. Leterrier, L. Medico, F. Demarco, J.-A. E. Manson, U. Betz, M. F. Escola, M. Kharrazi Olsson, F. Atamny, *Thin Solid Films* **2004**, *460*, 156.
[226] K. Nomura, T. Kamiya, H. Ohta, K. Ueda, M. Hirano, H. Hosono, *Appl. Phys. Lett.* **2004**, *85*, 1993.
[227] E. Fortunato, P. Barquinha, A. Pimentel, A. Goncalves, A. Marques, L. Pereira, R. Martins, *Adv. Mater.* **2005**, *17*, 590.
[228] G. Gruner, *Sci. Am.* **2007**, *296*, 76.
[229] Z. R. Li, H. R. Kandel, E. Dervishi, V. Saini, Y. Xu, A. R. Biris, D. Lupu, G. J. Salamo, A. S. Biris, *Langmuir* **2008**, *24*, 2655.
[230] D. H. Zhang, K. Ryu, X. L. Liu, E. Polikarpov, J. Ly, M. E. Tompson, C. W. Zhou, *Nano Lett.* **2006**, *6*, 1880.
[231] B. S. Kong, D. H. Jung, S. K. Oh, C. S. Han, H. T. Jung, *J. Phys. Chem. C* **2007**, *111*, 8377.
[232] H. Z. Geng, K. K. Kim, C. Song, N. T. Xuyen, S. M. Kim, K. A. Park, D. S. Lee, K. H. An, Y. S. Lee, Y. Chang, Y. J. Lee, J. Y. Choi, A. Benayad, Y. H. Lee, *J. Mater. Chem.* **2008**, *18*, 1261.
[233] H. Z. Geng, K. K. Kim, K. P. So, Y. S. Lee, Y. Chang, Y. H. Lee, *J. Am. Chem. Soc.* **2007**, *129*, 7758.
[234] M. Kaempgen, M. Lebert, M. Haluska, N. Nicoloso, S. Roth, *Adv. Mater.* **2008**, *20*, 616.
[235] A. A. Green, M. C. Hersam, *Nano Lett.* **2008**, *8*, 1417.
[236] E. Artukovic, M. Kaempgen, D. Hecht, S. Roth, G. Grüner, *Nano Lett.* **2005**, *5*, 757.
[237] K. Lee, Z. Wu, Z. Chen, F. Ren, S. J. Pearton, A. G. Rinzler, *Nano. Lett.* **2004**, *4*, 911.
[238] W. Yuan, L. B. Hu, Z. B. Yu, T. L. Lam, J. Biggs, S. M. Ha, D. J. Xi, B. Chen, M. K. Senesky, G. Gruner, Q. B. Pei, *Adv. Mater.* **2008**, *20*, 621.
[239] V. Jain, H. M. Yochum, R. Montazami, J. R. Heflin, L. B. Hu, G. Gruner, *J. Appl. Phys.* **2008**, *103*, 074504.
[240] L. B. Hu, G. Gruner, D. Li, R. B. Kaner, J. Cech, *J. Appl. Phys.* **2007**, *101*, 016102.
[241] L. B. Hu, G. Gruner, J. Gong, C. J. Kim, B. Hornbostel, *Appl. Phys. Lett.* **2007**, *90*, 093124.
[242] G. Thomas, *Nature* **1997**, *389*, 907.
[243] Q. Cao, Z. T. Zhu, M. G. Lemaitre, M. G. Xia, M. Shim, J. A. Rogers, *Appl. Phys. Lett.* **2006**, *88*, 113511.
[244] S. K. Kim, S. H. Ju, J. H. Back, Y. Xuan, P. D. Ye, M. Shim, D. B. Janes, S. Mohammadi, *Adv. Mater.* **2008**, DOI:10.1002/adma.200801032.
[245] R. L. Hoffman, B. J. Norris, J. F. Wager, *Appl. Phys. Lett.* **2003**, *82*, 733.
[246] R. A. Hatton, A. J. Miller, S. R. P. Silva, *J. Mater. Chem.* **2008**, *18*, 1183.
[247] A. R. Schlatmann, D. W. Floet, A. Hilberer, F. Garten, P. J. M. Smulders, T. M. Klapwijk, G. Hadziioannou, *Appl. Phys. Lett.* **1996**, *69*, 1764.
[248] J. Ni, H. Yan, A. Wang, Y. Yang, C. L. Stern, A. W. Metz, S. Jin, L. Wang, T. J. Marks, J. R. Ireland, C. R. Kannewurf, *J. Am. Chem. Soc.* **2005**, *127*, 5613.
[249] B. Shan, K. J. Cho, *Phys. Rev. Lett.* **2005**, *94*, 236602.
[250] J. Li, L. Hu, L. Wang, Y. Zhou, G. Gruner, T. J. Marks, *Nano Lett.* **2006**, *6*, 2472.
[251] M. W. Rowell, M. A. Topinka, M. D. McGehee, H. J. Prall, G. Dennler, N. S. Sariciftci, L. B. Hu, G. Gruner, *Appl. Phys. Lett.* **2006**, *88*, 233506.
[252] J. van de Lagemaat, T. M. Barnes, G. Rumbles, S. E. Shaheen, T. J. Coutts, C. Weeks, I. Levitsky, J. Peltola, P. Glatkowski, *Appl. Phys. Lett.* **2006**, *88*, 233503.
[253] K. Besteman, J. O. Lee, F. G. M. Wiertz, H. A. Heering, C. Dekker, *Nano Lett.* **2003**, *3*, 727.
[254] Q. F. Pengfei, O. Vermesh, M. Grecu, A. Javey, O. Wang, H. J. Dai, S. Peng, K. J. Cho, *Nano Lett.* **2003**, *3*, 347.
[255] B. Mahar, C. Laslau, R. Yip, Y. Sun, *IEEE Sens. J.* **2007**, *7*, 266.
[256] E. S. Snow, J. P. Novak, M. D. Lay, F. K. Perkins, *Appl. Phys. Lett.* **2004**, *85*, 4172.
[257] E. S. Snow, F. K. Perkins, E. J. Houser, S. C. Badescu, T. L. Reinecke, *Science* **2005**, *307*, 1942.
[258] E. S. Snow, F. K. Perkins, J. A. Robinson, *Chem. Soc. Rev.* **2006**, *35*, 790.
[259] C. Staii, A. T. Johnson, *Nano Lett.* **2005**, *5*, 1774.
[260] J. P. Novak, E. S. Snow, E. J. Houser, D. Park, J. L. Stepnowski, R. A. McGill, *Appl. Phys. Lett.* **2003**, *83*, 4026.
[261] J. A. Robinson, E. S. Snow, F. K. Perkins, *Sens. Actuator A-Phys.* **2007**, *135*, 309.
[262] L. Senesac, T. G. Thundat, *Mater. Today* **2008**, *11*, 28.
[263] J. A. Robinson, E. S. Snow, S. C. Badescu, T. L. Reinecke, F. K. Perkins, *Nano Lett.* **2006**, *6*, 1747.
[264] A. Star, T. R. Han, J. C. P. Gabriel, K. Bradley, G. Gruner, *Nano Lett.* **2003**, *3*, 1421.
[265] E. S. Snow, F. K. Perkins, *Nano Lett.* **2005**, *5*, 2414.
[266] S. Mubeen, T. Zhang, B. Yoo, M. A. Deshusses, N. V. Myung, *J. Phys. Chem. C* **2007**, *111*, 6321.
[267] Y. Sun, H. H. Wang, *Adv. Mater.* **2007**, *19*, 2818.
[268] Y. Sun, H. H. Wang, *Appl. Phys. Lett.* **2007**, *90*, 213107.
[269] Y. G. Sun, H. H. Wang, M. G. Xia, *J. Phys. Chem. C* **2008**, *112*, 1250.
[270] O. Kuzmych, B. L. Allen, A. Star, *Nanotechnology* **2007**, *18*, 375502.
[271] Y. J. Lu, J. Li, J. Han, H. T. Ng, C. Binder, C. Partridge, M. Meyyappan, *Chem. Phys. Lett.* **2004**, *391*, 344.
[272] A. Star, T. R. Han, V. Joshi, J. C. P. Gabriel, G. Gruner, *Adv. Mater.* **2004**, *16*, 2049.
[273] A. Star, V. Joshi, S. Skarupo, D. Thomas, J. C. P. Gabriel, *J. Phys. Chem. B* **2006**, *110*, 21014.
[274] C. Y. Lee, R. Sharma, A. D. Radadia, R. I. Masel, M. S. Strano, *Angew. Chem. Int. Ed.* **2008**, *47*, 5018.
[275] B. L. Allen, P. D. Kichambare, A. Star, *Adv. Mater.* **2007**, *19*, 1439.
[276] G. Gruner, *Anal. Bioanal. Chem.* **2006**, *384*, 322.
[277] K. Bradley, M. Briman, A. Star, G. Gruner, *Nano Lett.* **2004**, *4*, 253.
[278] A. Star, E. Tu, J. Niemann, J. C. P. Gabriel, C. S. Joiner, C. Valcke, *Proc. Natl. Acad. Sci. U. S. A.* **2006**, *103*, 921.
[279] E. L. Gui, L. J. Li, P. S. Lee, A. Lohani, S. G. Mhaisalkar, Q. Cao, S. J. Kang, J. A. Rogers, N. C. Tansil, Z. Q. Gao, *Appl. Phys. Lett.* **2006**, *89*, 232104.
[280] I. Heller, A. M. Janssens, J. Mannik, E. D. Minot, S. G. Lemay, C. Dekker, *Nano Lett.* **2008**, *8*, 591.

[281] E. L. Gui, L. J. Li, K. K. Zhang, Y. P. Xu, X. C. Dong, X. N. Ho, P. S. Lee, J. Kasim, Z. X. Shen, J. A. Rogers, S. G. Mhaisalkar, *J. Am. Chem. Soc.* **2007**, *129*, 14427.
[282] X. W. Tang, S. Bansaruntip, N. Nakayama, E. Yenilmez, Y. L. Chang, Q. Wang, *Nano Lett.* **2006**, *6*, 1632.
[283] H. R. Byon, H. C. Choi, *J. Am. Chem. Soc.* **2006**, *128*, 2188.
[284] X. C. Dong, C. M. Lau, A. Lohani, S. G. Mhaisalkar, J. Kasim, Z. X. Shen, X. N. Ho, J. A. Rogers, L. J. Li, *Adv. Mater.* **2008**, *20*, 2389.
[285] R. J. Chen, Y. Zhang, D. Wang, H. Dai, *J. Am. Chem. Soc.* **2001**, *123*, 3838.
[286] C. Li, M. Curreli, H. Lin, B. Lei, F. N. Ishikawa, R. Datar, R. J. Cote, M. E. Thompson, C. W. Zhou, *J. Am. Chem. Soc.* **2005**, *127*, 12484.
[287] R. J. Chen, S. Bangsaruntip, K. A. Drouvalakis, N. W. S. Kam, M. Shim, Y. M. Li, W. Kim, P. J. Utz, H. J. Dai, *Proc. Natl. Acad. Sci. U. S. A.* **2003**, *100*, 4984.
[288] Y. L. Zhao, L. B. Hu, J. F. Stoddart, G. Grüner, *Adv. Mater.* **2008**, *20*, 1910.
[289] H. M. So, K. Won, Y. H. Kim, B. K. Kim, B. H. Ryu, P. S. Na, H. Kim, J. O. Lee, *J. Am. Chem. Soc.* **2005**, *127*, 1906.
[290] H. M. So, D. W. Park, E. K. Jeon, Y. H. Kim, B. S. Kim, C. K. Lee, S. Y. Choi, S. C. Kim, H. Chang, J. O. Lee, *Small* **2008**, *4*, 197.
[291] H. Yoon, J. H. Kim, N. Lee, B. G. Kim, J. Jang, *ChemBioChem* **2008**, *9*, 634.
[292] R. H. Reuss, D. G. Hopper, J. G. Park, *MRS Bull.* **2006**, *31*, 447.
[293] S. Lee, B. Koo, J. G. Park, H. Moon, J. Hahn, J. M. Kim, *MRS Bull.* **2006**, *31*, 455.
[294] P. van der Wilt, M. G. Kane, A. B. Limanov, A. H. Firester, L. Goodman, J. Lee, J. Abelson, A. M. Chitu, J. S. Im, *MRS Bull.* **2006**, *31*, 461.
[295] E. S. Snow, J. P. Novak, M. D. Lay, E. H. Houser, F. K. Perkins, P. M. Campbell, *J. Vac. Sci. Technol. B* **2004**, *22*, 1990.
[296] Y. S. Min, E. J. Bae, B. S. Oh, D. Kang, W. Park, *J. Am. Chem. Soc.* **2005**, *127*, 12498.
[297] B. J. Yoon, E. H. Hong, S. E. Jee, D. M. Yoon, D. S. Shim, G. Y. Son, Y. J. Lee, K. H. Lee, H. S. Kim, C. G. Park, *J. Am. Chem. Soc.* **2005**, *127*, 8234.
[298] K. Bradley, J.-C. P. Gabriel, G. Grüner, *Nano. Lett.* **2003**, *3*, 1353.
[299] D. R. Hines, S. Mezhenny, M. Breban, E. D. Williams, V. W. Ballarotto, G. Esen, A. Southard, M. S. Fuhrer, *Appl. Phys. Lett.* **2005**, *86*, 163101.
[300] X. L. Liu, S. Han, C. W. Zhou, *Nano Lett.* **2006**, *6*, 34.
[301] M. H. Yoon, A. Facchetti, T. J. Marks, *Proc. Natl. Acad. Sci. U. S. A.* **2005**, *102*, 4678.
[302] A. Robert-Peillard, S. V. Rotkin, *IEEE Trans. Nanotechnol.* **2005**, *4*, 284.
[303] J. S. Lee, S. Ryu, K. Yoo, I. S. Choi, W. S. Yun, J. Kim, *J. Phys. Chem. C* **2007**, *111*, 12504.
[304] E. S. Snow, P. M. Campbell, M. G. Ancona, J. P. Novak, *Appl. Phys. Lett.* **2005**, *86*, 033105.
[305] J. Xiang, W. Lu, Y. J. Hu, Y. Wu, H. Yan, C. M. Lieber, *Nature* **2006**, *441*, 489.
[306] R. Nouchi, H. Tomita, A. Ogura, H. Kataura, M. Shiraishi, *Appl. Phys. Lett.* **2008**, *92*, 253507.
[307] E. Menard, M. A. Meitl, Y. G. Sun, J. U. Park, D. J. L. Shir, Y. S. Nam, S. Jeon, J. A. Rogers, *Chem. Rev.* **2007**, *107*, 1117.
[308] R. Parashkov, E. Becker, T. Riedl, H. H. Johannes, W. Kowalsky, *Proc. IEEE* **2005**, *93*, 1321.
[309] M. Chason, P. W. Brazis, H. Zhang, K. Kalyanasundaram, D. R. Gamota, *Proc. IEEE* **2005**, *93*, 1348.
[310] D. Y. Khang, H. Q. Jiang, Y. Huang, J. A. Rogers, *Science* **2006**, *311*, 208.
[311] D. H. Kim, J. H. Ahn, W. M. Choi, H. S. Kim, T. H. Kim, J. Z. Song, Y. G. Y. Huang, Z. J. Liu, C. Lu, J. A. Rogers, *Science* **2008**, *320*, 507.
[312] Y. G. Sun, W. M. Choi, H. Q. Jiang, Y. G. Y. Huang, J. A. Rogers, *Nat. Nanotechnol.* **2006**, *1*, 201.
[313] S. P. Lacour, J. Jones, S. Wagner, T. Li, Z. G. Suo, *Proc. IEEE* **2005**, *93*, 1459.
[314] T. Sekitani, Y. Noguchi, K. Hata, T. Fukushima, T. Aida, T. Someya, *Science* **2008**, *321*, 1468.
[315] H. C. Ko, M. P. Stoykovich, J. Z. Song, V. Malyarchuk, W. M. Choi, C. J. Yu, J. B. Geddes, J. L. Xiao, S. D. Wang, Y. G. Huang, J. A. Rogers, *Nature* **2008**, *454*, 748.
[316] C. Hierold, A. Jungen, C. Stampfer, T. Helbling, *Sens. Actuator A-Phys.* **2007**, *136*, 51.
[317] T. W. Tombler, C. W. Zhou, L. Alexseyev, J. Kong, H. J. Dai, L. Lei, C. S. Jayanthi, M. J. Tang, S. Y. Wu, *Nature* **2000**, *405*, 769.
[318] H. Maune, M. Bockrath, *Appl. Phys. Lett.* **2006**, *89*, 173131.
[319] N. K. Chang, C. C. Su, S. H. Chang, *Appl. Phys. Lett.* **2008**, *92*, 063501.
[320] Z. H. Zhong, N. M. Gabor, J. E. Sharping, A. L. Gaeta, P. L. McEuen, *Nat. Nanotechnol.* **2008**, *3*, 201.
[321] J. Guo, S. Hasan, A. Javey, G. Bosman, M. Lundstrom, *IEEE Trans. Nanotechnol.* **2005**, *4*, 715.
[322] A. A. Pesetski, J. E. Baumgardner, S. V. Krishnaswamy, H. Zhang, J. D. Adam, C. Kocabas, T. Banks, J. A. Rogers, *Appl. Phys. Lett.* **2008**, *93*, 123506.
[323] C. Kocabas, H. S. Kim, T. Banks, J. A. Rogers, A. A. Pesetski, J. E. Baumgardner, S. V. Krishnaswamy, H. Zhang, *Proc. Natl. Acad. Sci. U. S. A.* **2008**, *105*, 1405.
[324] S. D. Li, Z. Yu, S. F. Yen, W. C. Tang, P. J. Burke, *Nano. Lett.* **2004**, *4*, 753.
[325] J. Chaste, L. Lechner, P. Morfin, G. Feve, T. Kontos, J. M. Berroir, D. C. Glattli, H. Happy, P. Hakonen, B. Placais, *Nano Lett.* **2008**, *8*, 525.
[326] S. Rosenblatt, H. Lin, V. Sazonova, S. Tiwari, P. L. McEuen, *Appl. Phys. Lett.* **2005**, *87*, 153111.
[327] D. Wang, Z. Yu, S. McKernan, P. J. Burke, *IEEE Trans. Nanotechnol.* **2007**, *6*, 400.
[328] A. Le Louarn, F. Kapche, J. M. Bethoux, H. Happy, G. Dambrine, V. Derycke, P. Chenevier, N. Izard, M. F. Goffman, J. P. Bourgoin, V. Derycke, P. Chenevier, N. Izard, M. F. Goffman, J. P. Bourgoin, *Appl. Phys. Lett.* **2007**, *90*, 233108.
[329] N. Chimot, V. Derycke, M. F. Goffman, J. P. Bourgoin, H. Happy, G. Dambrine, *Appl. Phys. Lett.* **2007**, *91*, 153111.
[330] C. Kocabas, S. Dunham, Q. Cao, K. Cimino, X. N. Ho, H. S. Kim, J. E. Baumgardner, A. A. Pesetski, H. Zhang, T. Banks, M. Feng, J. A. Rogers, **2008**, Unpublished results.
[331] J. E. Baumgardner, A. A. Pesetski, J. M. Murduck, J. X. Przybysz, J. D. Adam, H. Zhang, *Appl. Phys. Lett.* **2007**, *91*, 052107.
[332] C. Rutherglen, P. Burke, *Nano Lett.* **2007**, *7*, 3296.
[333] K. Jensen, J. Weldon, H. Garcia, A. Zettl, *Nano Lett.* **2007**, *7*, 3508.
[334] J. B. Cui, R. Sordan, M. Burghard, K. Kern, *Appl. Phys. Lett.* **2002**, *81*, 3260.
[335] M. S. Fuhrer, B. M. Kim, T. Durkop, T. Brintlinger, *Nano Lett.* **2002**, *2*,755.
[336] M. Radosavljevic, M. Freitag, K. V. Thadani, A. T. Johnson, *Nano Lett.* **2002**, *2*, 761.
[337] X. F. Duan, C. M. Niu, V. Sahi, J. Chen, J. W. Parce, S. Empedocles, J. L. Goldman, *Nature* **2003**, *425*, 274.
[338] R. S. Friedman, M. C. McAlpine, D. S. Ricketts, D. Ham, C. M. Lieber, *Nature* **2005**, *434*, 1085.
[339] F. Patolsky, G. Zheng, C. M. Lieber, *Nanomedicine* **2006**, *1*, 51.
[340] X. F. Duan, *MRS Bull.* **2007**, *32*, 134.
[341] D. V. Talapin, C. B. Murray, *Science* **2005**, *310*, 86.
[342] S. A. Stauth, B. A. Parviz, *Proc. Natl. Acad. Sci. U. S. A.* **2006**, *103*, 13922.
[343] D. H. Kim, J. H. Ahn, H. S. Kim, K. J. Lee, T. H. Kim, C. J. Yu, R. G. Nuzzo, J. A. Rogers, *IEEE Trans. Electron. Devices* **2008**, *29*, 73.
[344] Y. G. Sun, J. A. Rogers, *Adv. Mater.* **2007**, *19*, 1897.
[345] A. J. Baca, J. H. Ahn, Y. G. Sun, M. A. Meitl, E. Menard, H. S. Kim, W. M. Choi, D. H. Kim, Y. Huang, J. A. Rogers, *Angew. Chem. Int. Ed.* **2008**, *47*, 5524.
[346] G. Eda, G. Fanchini, M. Chhowalla, *Nat. Nanotechnol.* **2008**, *3*, 270.
[347] D. Li, R. B. Kaner, *Science* **2008**, *320*, 1170.
[348] X. L. Li, X. R. Wang, L. Zhang, S. W. Lee, H. J. Dai, *Science* **2008**, *319*, 1229.
[349] J. A. Rogers, *Nat. Nanotechnol.* **2008**, *3*, 254.
[350] M. J. Schultz, X. Y. Zhang, S. Unarunotai, D. Y. Khang, Q. Cao, C. J. Wang, C. H. Lei, S. MacLaren, J. Soares, I. Petrov, J. S. Moore, J. A. Rogers, *Proc. Natl. Acad. Sci. U. S. A.* **2008**, *105*, 7353.